NTC 2

EXPERIMENTAL STUDY OF THE STARTING PROCESS, FLOW DURATION, AND NOZZLE BOUNDARY LAYER IN A HIGH-ENTHALPY SHOCK TUNNEL

Prepared for:

NATIONAL AERONAUTICS AND SPACE ADMINISTRATION
GODDARD SPACE FLIGHT CENTER
GREENBELT, MARYLAND

MICHAEL G. DUNN

CONTRACT NO. NAS 5-9978
CAL REPORT NO. AI-2187-A-6
NOVEMBER 1967

CORNELL AERONAUTICAL LABORATORY, INC.
OF CORNELL UNIVERSITY, BUFFALO, N. Y. 14221

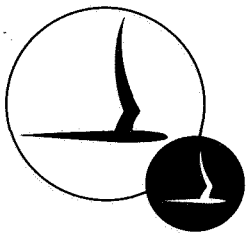

CORNELL AERONAUTICAL LABORATORY, INC.
BUFFALO, NEW YORK 14221

EXPERIMENTAL STUDY OF THE STARTING PROCESS, FLOW DURATION, AND NOZZLE BOUNDARY LAYER IN A HIGH-ENTHALPY SHOCK TUNNEL

CAL REPORT NO. AI-2187-A-6
CONTRACT NO. NAS 5-9978
NOVEMBER 1967

PREPARED FOR:
NATIONAL AERONAUTICS AND SPACE ADMINISTRATION
GODDARD SPACE FLIGHT CENTER
GREENBELT, MARYLAND

PREPARED BY: Michael G. Dunn
Michael G. Dunn

APPROVED BY: J. Gordon Hall
J. Gordon Hall
Head, Aerodynamic
Research Department

FOREWORD

The work described in this report was sponsored by the National Aeronautics and Space Administration, Goddard Space Flight Center, under Contract NAS 5-9978.

The author wishes to acknowledge Drs. J.G. Hall and T.J. Falk for their discussions during the course of this work.

ABSTRACT

Studies of the starting process and boundary-layer growth have been conducted in the conical nozzle of a reflected-shock tunnel using air as the test gas. These experiments were performed at shock-tube Mach numbers of 16.5 and 11.6, with corresponding initial driven-tube pressures of 0.5 and 10.0 mm Hg respectively. The ratio of the throat diameter to the shock-tube diameter was approximately 0.1. The time required to establish uniform flow in the nozzle was found to increase approximately linearly with axial distance from the throat. The duration of uniform flow was determined at several locations using microwave-interferometer, radiation-intensity, and pitot-pressure measurements.

The boundary-layer displacement-thickness growth on the nozzle wall was determined for both of the aforementioned experimental conditions using the measured velocity and density profiles. Good agreement was achieved between measured and theoretical pitot-pressures at comparable inviscid area ratios. In the experiment using the higher driven-tube pressure the measured wall static pressure agreed well with calculated values at the nozzle center line. However, in the case of the lower driven pressure, comparison of the measured wall static pressure with the theoretical value implied the existence of a substantial pressure gradient normal to the wall.

A summary of experiments conducted under other support to ascertain the range of validity of the equilibrium-interface concept as used in shock-tunnel operation is also presented. The test gas in these experiments was either air or nitrogen, and the driver gas was either hydrogen or helium. The driven-tube initial pressure was held fixed at 10.0 mm Hg and the Mach number varied from 7.3 to 12.2. The composition of the driver gas was found to be particularly important. With hydrogen used as the driver gas the increased enthalpy levels implied by the pressure data in the equilibrium interface region were apparently not achieved. With helium used as the driver gas the results suggested that the equilibrium-interface concept may be valid at substantially over-tailored incident-shock Mach numbers.

TABLE OF CONTENTS

TABLE OF CONTENTS (Cont.)

LIST OF ILLUSTRATIONS

LIST OF ILLUSTRATIONS (CONT.)

1. INTRODUCTION

The research reported here was motivated by an interest at Cornell Aeronautical Laboratory in the use of the shock-tunnel to study reaction-rate constants for nonequilibrium electron-recombination processes in an expanding flow environment. The purpose of this report, is to discuss the studies of the nozzle starting process and sidewall boundary-layer growth that were necessarily conducted prior to measurement of the reaction-rate constants. The starting-process data are important for choosing the proper test time out of the total run time. The boundary-layer data are important for understanding the inviscid gasdynamics of the flow.

Knowledge of the uniformity of the shock-tube flow is also of importance to the study of nozzle flows, since it is the reflected-shock processed gas that ultimately expands in the nozzle and becomes the test gas. Studies aimed at obtaining this information have previously been performed in the shock tube used here, and are reported in Reference 1 for incident-shock Mach numbers comparable to those of interest in this work.

The present experiments were conducted in a 13°-half-angle nozzle having a horizontal axis collinear with that of the shock tube. The test gas after having been processed by both the incident and reflected shocks enters the nozzle through a throat of diameter equal to 0.1 of the driven-tube inside diameter. Two experimental conditions were investigated in detail. In the first of these, the incident-shock Mach number (The Mach number discussed throughout this report is that measured near the shock-tube end wall) was 16.5 and the initial driven tube pressure was 0.5-mm Hg air. For the second condition, the incident-shock Mach number was 11.6 and the initial driven-tube pressure was 10.0-mm Hg air.

Several authors, References 2-9, have studied the flow phenomena associated with the process of starting a hypersonic shock-tunnel nozzle. References 2 and 3 present experimental results applicable to a non-reflected shock tunnel.

References 4 and 5 contain theoretical treatments of the starting process for this type of shock tunnel whereas Reference 7 is a similar study for a reflected shock tunnel. Limited experimental data are presented in References 6,8 and 9 for the starting process in reflected-shock tunnels. In the present experiments a more detailed study of the starting process has been made in that measurements of radiation intensity, phase shift and attenuation of microwave energy, sidewall pressure, pitot pressure, and stagnation-point heat-transfer rate have been obtained at several axial locations in the nozzle. Of these diagnostic techniques the radiation intensity and microwave interferometer measurements were found to be the most sensitive indicators of the onset of uniform nozzle flow. The theoretical calculations of C.E. Smith[7] were performed for a shock-tunnel geometry similar to that used here. For this reason his model of the starting process was used to aid in interpreting the experimental data.

The nozzle boundary-layer was investigated with the aid of radial surveys of pitot pressure and stagnation-point heat-transfer rate at several axial locations in the nozzle. These measurements were used to deduce the local velocity and density relative to the corresponding values on the nozzle center-line and the experimentally determined profiles were used to calculate the appropriate boundary-layer displacement thickness. Several authors[10-20] have proposed techniques that may be used to calculate boundary-layer growth on the wall of a conical nozzle and the present results could be used to test these techniques. However, the major emphasis of this report has been placed on the experimental measurements with only a limited comparison with theory. Two particular prediction techniques, described in References 11 and 14, have been selected as typical and the experimentally determined boundary-layer and displacement thicknesses are compared with these.

A brief review is presented of shock-tunnel experiments conducted under other support[21] to investigate the feasibility of achieving enthalpy levels greater than those that can be achieved at the tailored-interface Mach number, the condition at which the shock wave reflected from the end wall passes through the interface without reflection. For shock-wave Mach numbers greater than those for which the interface is tailored, it has been suggested by

Hertzberg, et al.[22] that after the initial shock reflection from the interface, subsequent reflections are sufficiently weak so that the remaining compression is isentropic as the interface is brought to rest. This latter region has been termed the equilibrium-interface region. Copper[23,24] has made pressure, heat-transfer rate, and gas sampling measurements in a nozzle which suggested the validity of this concept. The same diagnostic techniques used in the starting-process studies described earlier in this section were used to investigate the possibilities of realizing these increased enthalpy levels. Experiments were conducted for Mach numbers ranging from 7.3 to 12.2 with either air or nitrogen as the driven gas. The driver gas was either heated hydrogen or heated helium. The results of the equilibrium-interface experimental program were not encouraging. With hydrogen as the driver gas only a small enthalpy increase was obtainable in the equilibrium interface region. With helium as the driver gas the enthalpy levels in the equilibrium-interface region appeared to be greater than those immediately after shock reflection. However, these increased enthalpy levels were significantly less than those attainable in the reflected-shock region with a hydrogen driver.

In Section 2 the experimental apparatus and types of measurements taken in the shock tube and the nozzle are described in detail. The test results relating to the nozzle starting process duration of uniform nozzle flow, and boundary-layer growth are described in Sections 3,4,5, and 6 respectively. Measurements obtained in the equilibrium-interface region are discussed in Section 7. Typical data records pertinent to each of these subjects are also presented.

2. EXPERIMENTAL APPARATUS AND TECHNIQUE

A pressure-driven shock tube was used to produce a reservoir of high-temperature gas which was subsequently expanded in a conical nozzle. In the shock tube visible and near infrared radiation intensity, pressure, and sidewall temperature were measured. Measurements taken in the nozzle included electron density, visible radiation intensity, pitot and sidewall-static pressure, and stagnation-point heat-transfer rate. In the following paragraphs, the shock tube, the nozzle, and the type of instrumentation utilized to make measurements in each flow region are briefly described.

2.1 Shock-Tube and Nozzle Design and Operation

The shock tube utilized in this work is pressure driven and has a three-inch inside-diameter driver tube which is 9.0 ft. in length (see Figure 1). The driven tube is 98 ft. long and has a six-inch inside diameter. Provision is included for heating the driver gas to a maximum temperature of 760°F. The maximum driver pressure is 15,000 psi. Diaphragms initially separating the driver and driven tubes are ruptured using a double-diaphragm technique. The last two feet of the driven tube is essentially an instrumentation section which has a total of thirteen observation ports within 5 3/4-inches from the end wall and two at the end wall. The remaining portion of the driven tube has diametrically opposed observation ports located at axial intervals of two and four feet.

The shock-wave velocity is obtained over the last 18.6 feet of driven tube using thin-film temperature gauges mounted flush with the wall. The first four intervals are approximately 4 ft. and the last interval is approximately 2.6 ft. Electronic counters, started and stopped by signals from the thin-film gauges, are used to measure the time elapsed for shock-wave passage between stations. The last thin-film gauge is located 3 1/4-inches from the driven-tube end wall.

A detailed view of the nozzle throat design and appropriate dimensions is also presented in Figure 1. The entrance to the nozzle throat was less than one throat diameter (0.591 inches) in length. The diameter of the entrance to the throat was only slightly greater than the throat diameter as is shown in Figure 1. Beyond the throat the passage diverges rather slowly and becomes tangent to the nozzle wall at a location 2.75-inches downstream. A 0.002-inch-thick mylar diaphragm is used to separate the driven tube from the nozzle thus permitting evacuation of the nozzle while the driven tube is loaded.

The conical nozzle used in these experiments has a half-angle of 13° and is constructed of Fiberglas. The exit diameter of the nozzle is approximately 35 inches and the over-all length is approximately 77 inches. The nozzle has 26 instrumentation ports at axial intervals of 10.0-inches with the first set located 11.5-inches from the throat. The first and last stations have three ports whereas the intermediate locations each have four ports located on the horizontal and vertical axis. The instrumentation ports are large enough to contain the microwave interferometer horns. The nozzle is initially evacuated to a pressure of approximately 10^{-3} torr. The leak rate was such that at the time of driven-tube diaphragm rupture, the pressure in the nozzle was of the order of 1.0 to 10 microns.

2.2 Shock-Tube Instrumentation

2.2.1 Radiation-Intensity

Radiation intensity behind the incident shock was measured with an RCA 1P28 photomultiplier tube which is sensitive in the spectral region 0.2 to 0.6 microns. The photomultiplier tube viewed the plasma through a teflon tube, 1/16-inch inside diameter by 3-inches in length which terminated at a 1/8-inch-thick sapphire optical window in the shock-tube wall.

Measurements of radiation intensity in the spectral range 0.35 to 1.13 microns were made in the reflected-shock region looking normal

and parallel to the tube axis. These measurements were taken at 3/4-and 3 1/4-inches from the end wall and at the end wall respectively. Silicon photodiodes (EGG model SD-100) were used to make these measurements. These detectors also viewed the reflected-shock processed gas through a teflon tube, 1/16-inch-inside diameter by 3-inches in length, terminating at a 1/8-inch-thick sapphire window.

2.2.2 Pressure

A Kistler 603-A pressure transducer was mounted two feet upstream of the photomultiplier tube. The transducer was coated with an insulating compound to reduce its temperature sensitivity. Experiments were performed to confirm that this coating had no effect on the response time of the instrument.

The pressure transducers used in the reflected-shock region were shock-mounted Kistler 603-A transducers. Measurements were made of end-wall pressure, and sidewall pressure at 3/4- and 3 1/4-inches from the end wall.

2.2.3 Wall-Temperature and Heat-Transfer

Standard thin-film platinum gauges were used to measure the sidewall temperature behind the incident shock. Heat-transfer rates were determined from the surface-temperature measurements using the analog network suggested by Skinner.[25]

2.3 Nozzle Instrumentation

2.3.1 Radiation-Intensity

Radiation-intensity measurements were made at several locations in the nozzle using RCA 1P28 photomultiplier tubes. The photomultiplier tube

viewed the plasma normal to the nozzle axis through teflon tubes and sapphire windows similar to those used for the shock-tube measurements.

2.3.2 Microwave-Interferometer

Microwave interferometers with operating frequencies of 142, 35, and 17 GHz were used in the nozzle to aid in the understanding of the nozzle gasdynamics and to measure the local electron density. The interferometer measurements were obtained at several axial locations. The microwave energy enters and leaves the plasma via thin mylar (in the case of the 142 GHz interferometer) or quartz (in the case of the 35 and 17 GHz interferometers) windows which had a maximum diameter of 1.2 inches. The phase shift and attenuation of the transmitted signal are measured separately as are the incident and reflected power. Two interferometers 142 and 35 GHz, were operated at the same axial distance from the throat to obtain a comparative check on the two systems.

2.3.3 Pressure

Pitot-pressure surveys normal to the nozzle axis were obtained at axial distances from the throat of 28, 38, 48 and 68 inches using flush-diaphragm piezoelectric pressure transducers.* These instruments have 1/4-inch diameter diaphragms, a sensitivity nominally equal to 1/2-volt per psi, and a nominal response time of 40 μ sec. They were flush mounted in a holder which was 1/2-inch in diameter and approximately 3 inches in length. From five to eight probes were mounted in each rake and were aligned with the nozzle throat.

The pressure transducers described in the preceding paragraph were also used to measure sidewall static pressure at each of the nozzle instrumentation stations. The transducer diaphragms were mounted flush with the nozzle wall.

---

*This flush-diaphragm transducer was developed earlier at CAL by Mr. R. MacArthur of the Hypersonic Facilities Department.

2.3.4 Stagnation-Point Heat-Transfer Rate

Stagnation-point heat-transfer rate distributions normal to the nozzle axis were obtained at axial locations of 11, 21, 31, 41, 51, and 71-inches from the throat using twelve thin-film platinum gauges and the analog network mentioned in Section 2.2. The gauges were fired on pyrex rod, the diameter of the rod depending upon the particular axial location. At the 11-inch location the rod diameter was 1/8 inch, at the 21-inch location it was 5/16 inch, and at all other locations the rod diameter was 1/2 inch. At the first two axial locations the gauges were nominally 0.10-inches in length and 0.03-inches in width. The thin-film gauges at axial locations of 31-inches and greater downstream were nominally 0.18 inches in length and 0.04 inches in width. Each gauge was calibrated prior to the experiment. Good agreement was obtained between the room temperature resistance of the gauges measured after the experiment and the pre-experiment value.

2.3.5 Langmuir-Probe

Langmuir probes were used in the nozzle to ascertain the uniformity of the fluid flow. The tips of the probes were located 26.4 inches downstream of the throat. The probes were 0.004 inches in diameter and approximately 0.20-inches long. Three probes were mounted in a sharp-wedge model at this axial location. The period of uniform flow was established for each experimental condition by using a fixed bias voltage on the probes. Having done this, the bias voltage on the centerline probe was swept from -10 to +10 volts in a period of time somewhat less than the corresponding duration of uniform flow. The two remaining probes were held at fixed bias voltage so that a current-voltage consistency check could be made on the swept probe.

3. NOZZLE STARTING-PROCESS MEASUREMENTS

The nozzle starting process discussed in this section and boundary-layer growth experiments discussed in Sections 5 and 6 were conducted at two experimental conditions and consisted of approximately 100 separate experiments. Both the quantitative and qualitative characteristics of the experimental data were reproducible. At the first of these experimental conditions the test gas was air at an initial driven-tube pressure of 0.50 mm Hg and the nominal incident-shock Mach number was 16.5. This shock-wave velocity and initial pressure resulted in a reflected-shock reservoir temperature of 7800°K, computed using the results of Feldman,[26] and a measured reflected-shock reservoir pressure of 3.74 atmospheres. The measured pressure was within a few percent of the theoretical value of Reference 26. The second experimental condition consisted of air at an initial driven-tube pressure of 10.0 mm Hg and a nominal incident-shock Mach number of 11.6. For this case, the computed reflected-shock reservoir temperature was 6830°K and the measured reflected-shock reservoir pressure was 25 atmospheres. Once again, the measured pressure was in excellent agreement with the theoretical value.

The results of the study described in the preceding paragraphs are discussed in the remainder of the text.

3.1 Shock-Tube Flow Conditions

Knowledge of conditions behind the incident shock and in the reflected-shock reservoir of the shock-tube is fundamental to the interpretation of the gasdynamics of the nozzle flow. Experiments have been performed in the shock tube used here in order to obtain this information and the results are reported in Reference 1. The results of that work which are particularly relevant to the current study are briefly summarized in the following paragraph.

The measured incident-shock test times for both laminar and turbulent boundary-layer flow were found to be in excellent agreement with the theories of Mirels.[27,28] Microwave interferometer measurements indicated that the electron density behind the incident shock was in good agreement with the theoretical equilibrium value. These results suggested the absence of any easily ionizable impurities and was particularly important to the success of the electron-recombination measurements to be conducted in the nozzle. In addition, the reflected-shock laminar boundary-layer interaction[29] is believed to have an influence on the sidewall pressure, but negligible effect on the uniformity of the inviscid reflected-shock gasdynamics. It is not the intention to imply that the interaction does not have an influence on the time duration of the uniform reservoir.

3.2 Model of Starting Process

Wave diagrams for the starting process in shock tunnels have been given by several authors.[2-9] As previously noted, much of this work has been directly applicable to non-reflected shock tunnels. In some cases[2,3] the initial pressure in the shock tube and in the nozzle were equal. The work of Glick, et al.[4] was directed primarily towards the case in which the nozzle length was short compared with the test-section length. The studies of References 6-9 are more closely related to the present case.

The model used by C.E. Smith[7] in his theoretical study of the reflected shock-tunnel starting process is shown in Figure 2. The early-time flow near the diaphragm is similar to shock-tube flow in that there is a primary shock, contact surface and expansion fan. The expansion fan is followed by the quasi-steady flow of gas in which shock-tunnel experiments are normally performed.

In the present experiments the nozzle is initially evacuated to a very low pressure so that behind the primary shock one would expect a high temperature, low-density flow followed by a lower-temperature but higher density flow between the contact surface and the tail of the expansion fan. Through the

expansion fan the pressure, density and temperature of the gas must adjust to the conditions associated with the quasi-steady flow.

Smith's results indicate that the primary shock and the tail of the expansion fan would pass a given nozzle location in a time relatively short compared to the time required for passage of the expansion fan.

The velocity of the primary shock, which strongly depends upon the initial temperature and pressure ratio across the diaphragm, decreases as it moves down the nozzle because of the increasing cross-sectional area. Friedman[30] explains that this interaction results in the appearance of a secondary shock of increasing strength which is initially located at the tail of the expansion fan. The implication of his work is that this shock must eventually appear regardless of the initial nozzle pressure. The secondary shock had been detected experimentally several years before Friedman's work by Parks[3] and Hall[31] for the case of the nozzle and driven tube initially at the same pressure.

3.3 Pitot-Pressure and Stagnation-Point Heat-Transfer Rate Measurements

Pitot-pressure and stagnation-point heat-transfer rate measurements were obtained at several axial locations as the initial step in attempting to understand the gasdynamics of the nozzle flow. For the purposes of this report, the starting-process discussion will be confined to a presentation of the results obtained for an initial driven-tube pressure of 0.5 mm Hg air. The results obtained for an initial pressure of 10.0 mm Hg are similar and thus are not discussed. Figure 3 presents pitot-pressure results obtained at 28, 38, 48 and 68-inches from the nozzle throat which illustrate a uniform pressure increase to a pressure plateau. The character of this pressure increase is qualitatively consistent with that expected through an expansion fan and there are no obvious indications of the shocks or interface preceding the fan. It will be shown later in this section that the values of the pressure plateaus shown on Figures 3 (a), (b), and (c) are in excellent agreement with the pitot

pressures calculated from a one-dimensional, steady-flow solution of an expanding gas. The time required to achieve a uniform pressure level after the arrival of the initial disturbances is denoted as nozzle starting time and is shown in Figure 3. Figures 3 (b), (c) and (d) are all triggered from the same location so that time events are directly comparable on these records.

The character of the pitot-pressure measurements is typical of an expansion fan suggesting that this diagnostic does not record the presence of the primary shock, contact surface or a rearward-facing secondary shock. Because of the low initial pressure in the nozzle the pressure rise across the primary shock can be shown to be too low to be recorded on the pressure scale of Figure 3. The secondary shock would not appear if the tail of the expansion fan and the secondary shock are close together in time, because the response time of the pressure transducers may not be sufficient to resolve the two events.

Pitot-pressure measurements could not be obtained at locations closer to the throat than 28-inches. However, stagnation-point heat-transfer rate measurements were obtained nearer to the throat and typical results are shown in Figure 4 for axial locations of 11, 21, 41, and 51-inches. Figures 4 (b), (c) and (d) were all triggered from the same location. However, these records were not triggered from the same location as Figure 3 (b), (c) and (d). The time required to achieve uniform heat-transfer rate is marked on the data records as nozzle starting time. The starting times measured from the stagnation-point heat-transfer data are in good agreement with those obtained from the pitot-pressure results.

3.4 Sidewall-Pressure Measurements in Nozzle

Sidewall-pressure measurements were obtained at axial locations of 11.5, 21.5, 31.5, 41.5 and 51.5-inches from the nozzle throat. Figure 5 is typical of such a measurement obtained at 21.5-inches. The initial 20-microseconds of pressure rise is rapid and is followed by a more gradual but uniform increase to a uniform pressure level. It is possible that the initial signal received by the sidewall pressure transducer is a result of the primary shock. The

static pressure behind the primary shock was computed for this experimental condition and found to be sufficient to provide a measurable signal at the transducer sensitivity being used. If the initial pressure disturbance is due to the primary shock, then the experimental data are consistent with Smith's[7] suggestion that the primary shock and the tail of the expansion fan are close together in time since the nozzle starting time deduced from these measurements is in good agreement with that obtained from the pitot-pressure measurements.

3.5 Microwave-Interferometer Measurements

Figure 6 presents a typical microwave-interferometer (142 GHz operating frequency) data record taken at 11.5-inches from the nozzle throat. The arrival of the initial disturbance is readily observed as a very sharp increase in the phase shift of the incident microwave energy which suggests a very rapid increase in the local electron density. Passage of the primary shock should not be observed by an interferometer operating at this frequency because of the low initial pressure in the nozzle which would result in a relatively low electron density between the primary shock and the contact surface. In any event, the time required to achieve a reasonably uniform electron-density level is apparent from this data record.

3.6 Radiation-Intensity Measurements

Radiation-intensity measurements obtained in the nozzle at axial locations of 11.5- and 21.5-inches from the throat are presented in Figure 7. The corresponding radiation-intensity data record obtained in the reflected-shock reservoir at 3/4- and 3 1/4-inches from the end wall are given in Figure 8. The reflected-shock radiation-intensity record indicates that the reservoir from which the test gas was expanding remained rather uniform for a period of approximately 130 μsec. The first measurable signal detected in radiation-intensity data records obtained in the nozzle and shown in Figure 7 (occurring at approximately 30 sec after sweep initiation) is not felt to be associated

with the starting process because this signal is recorded at the same time by all of the photomultiplier tubes independent of axial location. The starting process is observed as a large increase in radiation intensity followed by a marked relaxation to a plateau value. On the basis of these data records it is not possible to ascertain whether this sudden increase in radiation intensity is associated with the primary shock or the expansion fan. It is clear that through the expansion fan the temperature and density of the gas must increase. However, the sharp radiation-intensity decrease shown in Figure 7 cannot be explained by the expansion fan. Several experiments were conducted in an attempt to determine the cause of the radiation-intensity peak. The results of these experiments will be discussed in Section 3.8.

3.7 Comparison of Starting-Time Results

Before continuing the discussion of the radiation-intensity peak it is perhaps appropriate to compare the results obtained from the diagnostic techniques discussed in Sections 3.3 to 3.6. The indicated times of first disturbance obtained from the sidewall static-pressure and microwave-interferometer measurements are noted on the radiation-intensity data records of Figure 7 for comparison purposes. At all locations, the sidewall pressure data suggested earlier measureable signals than did the microwave interferometer, but later initial signals than the photomultiplier tubes. It is interesting to note that the first disturbance measured with the microwave interferometer occurred at a time approximately equal to that of the radiation-intensity peak.

The time required to establish uniform flow at a given nozzle location can be estimated by an integration of a $(u - a)$ wave where the values of u and a are obtained from a quasi steady-state calculation of the gasdynamic variables. Such a calculation has been performed and the times obtained by integrating the quantity $\tau = \int \frac{dx}{(u-a)}$ are shown on Figures 7(a) and (b). The calculated times required to achieve uniform flow are shown to be in reasonably good agreement with the beginning of uniform flow marked on the data records. Both real gas and boundary-layer influences were included in this calculation.

Figure 9 presents the axial variation of the time required to achieve uniform nozzle flow after arrival of the initial disturbance as obtained from the various diagnostic techniques discussed in the preceding paragraphs. The pitot pressure data suggest a significantly shorter time required to achieve uniform flow after arrival of the initial disturbance because this diagnostic tool fails to detect the primary shock and the contact surface as noted in Section 3.3. With this reservation, it is concluded that all of the diagnostic techniques discussed are effective for determining the nozzle starting time.

3.8 Influence of Nozzle Pressure on Starting Process

It was noted in Section 3.6 that experiments were conducted in an effort to determine the cause of the large radiation-intensity spike shown on Figure 7. Radiation-intensity measurements were performed to assess the influence of initial nozzle pressure and the influence of diaphragm particles on these data records. Diaphragm particles apparently were not responsible for the observed radiation-intensity spike since measurements obtained at comparable tube and nozzle conditions with and without the diaphragm gave similar results.

Figure 10 illustrates the influence of initial nozzle pressure on the magnitude of the radiation-intensity spike. Although the driven and driver-tube conditions are different from those of Figure 7 they are similar to those discussed later in this report and the data are considered to be representative of the nozzle gasdynamics discussed throughout this report. Comparison of Figures 10(a) and 10(b) indicates that the magnitude of the radiation-intensity spike is significantly influenced by the initial nozzle pressure. The exact source of the radiation-intensity spike cannot be identified from this result. However, since only the gasdynamic parameters between the primary and secondary shocks should have been altered by the increased pressure, it would appear that the radiation spike is associated with that region. Figure 10(a) illustrates what appears to be an expansion fan immediately following the radiation-intensity spike. In experiments conducted at higher initial nozzle pressures the initial

radiation-intensity tends to mask the expansion fan either because the secondary shock moves back into the fan or because of the larger spike signal coupled with the imperfect resolution of instrumentation. It is important to observe that the magnitude of the radiation intensity during that portion described as uniform flow was identical in both experiments. In addition, the duration of uniform flow is only slightly influenced by the initial nozzle pressure. The technique used to determine the nozzle starting time from the radiation-intensity data is illustrated on Figure 10.

4. DURATION OF UNIFORM NOZZLE FLOW

The duration of uniform flow in the nozzle has been deduced for the 0.5 mm Hg experiment from the radiation-intensity (Figures 7, 10), microwave-interferometer (Figure 6) and the pitot-pressure (Figure 3) measurements and the results are presented in Figure 11. The stagnation-point heat-transfer rate measurements presented in Figure 4 are not very useful for determining this quantity. Microwave-interferometer and radiation-intensity measurements, which are considered to be the most sensitive indicators of uniform flow, were difficult to obtain beyond 21.5-inches from the throat. Pitot-pressure data on the other hand could not be obtained upstream of 28 inches and there was no overlap of the pitot-pressure data with the radiation-intensity and interferometer data. There is a suggestion in Figure 11 that the duration of uniform flow as deduced from pitot-pressure measurements may be significantly greater than the actual duration. The results presented in Figure 11 indicate that in some cases the radiation-intensity measurement indicated a somewhat greater uniform-flow period than did the microwave interferometer. This is probably not a result of the accuracy of the two diagnostic tools but rather it is related to the degree of arbitratiness with which one chooses the end of the useful flow period.

For this experimental condition, all of the results obtained at 11.5 inches indicate that there is at least 60 μsec of uniform flow and at 21.5 inches there is at least 80 μsec of uniform flow. It is believed that at 50 inches the duration of uniform flow is on the order of 140 μsec rather than the period of 200 μsec suggested by the pitot pressure data.

4.1 Nozzle Measurements at Increased Driven-Tube Pressures

The experimental results discussed in the preceding sections were applicable to an initial driven-tube pressure of 0.50 mm Hg air and a nominal Mach number of 16.5. Similar measurements were obtained for an initial driven-tube pressure of 10.0 mm Hg air and a nominal Mach number of 11.6. The character

of the nozzle starting process determined using the same diagnostic techniques as previously described, was similar to that previously discussed.

Figure 12 presents a comparison of the reflected-shock radiation intensity, taken 3/4 and 3 1/4-inches from the shock-tube end wall, with radiation intensity measured in the nozzle at 21.5 inches from the throat. What appears to be a portion of the expansion fan can be seen on Figure 12 (b) and is followed by a uniform plateau of approximately 260 μsec duration which represents the test gas. An integration of (u - a) was also performed for this experimental condition in order to estimate the time at which uniform flow should be expected. The resulting time is noted on Figure 12 (b) and shown to be in good agreement with the beginning of the radiation-intensity plateau just discussed. This plateau in radiation intensity, representing the test time, is terminated by a large increase in intensity which was not observed at the previous experimental condition. In Figure 12 (b), the radiation-intensity increase that terminates the uniform-flow plateau attains a peak which is approximately 50 percent greater than the plateau value. The cause of this increasing radiation is not evident from the reflected-shock radiation-intensity record of Figure 12(a). However, the radiation-intensity recorded by the upper trace of Figure 12(a) is significantly different from the corresponding intensity recorded for the 0.5 mm Hg experiments shown in Figure 8. The principle difference between the reservoir radiation-intensity records is that the magnitude of the intensity decrease, which terminates the duration of the uniform reflected-shock period, does not fall to the base line but rather decreases by approximately 50 percent and then reaches another relatively constant value. It is not possible to determine from these radiation-intensity records the magnitude of the corresponding translational temperature decrease.

For many of the experiments conducted at 10.0 mm Hg, the uniform flow period in the nozzle was terminated by an even greater increase in radiation intensity than shown in Figure 12. Figure 13 represents a radiation-intensity record frequently obtained in the nozzle for the same driver and driven-tube conditions as Figure 12. The early time history of Figure 13(b) is similar to that presented in Figure 12(b) (notice that the sensitivity of the nozzle

radiation-intensity record has been increased from 2 mv/cm to 1 mv/cm), but duration of the test-time plateau is substantially decreased from approximately 260μsec to approximately 200μsec.

It should be noted that the driver-tube gas for all of the results presented above was hydrogen heated to 760°F and the driven-tube gas was air. The possibility of hydrogen combustion which, if no impurities were present, would probably not be detected by the photodiode in the reflected-shock reservoir cannot be ruled out. Significantly, these two distinctively different nozzle radiation-intensity records (Figure 12(b) and 13(b) were obtained with approximately equal regularity during the course of 35 experiments at this driver-and driven-tube condition. In an effort to determine the cause of this radiation-intensity spike, experiments were conducted with nitrogen as the driven-tube gas and hydrogen as the driver-tube gas. These experiments are discussed in more detail later in this report. However, the spike discussed above was not observed in the nitrogen experiments. It is thus possible that combustion may play a role in terminating the uniform nozzle flow. However, for the purposes of the planned reaction-rate constant measurements, 200μsec of uniform flow is more than sufficient time for obtaining the necessary microwave-interferometer data. Thus the cause of the radiation-intensity spike that terminates the uniform flow was not investigated further.

4.2 Radiation-Intensity Measurements in Reflected-Shock Reservoir

The question of the reproducibility of reflected-shock conditions and the influence of the nozzle throat design on the reflected-shock test time is a relevant one. The reflected-shock radiation-intensity measurements presented in Figures 8, 12, 13 were obtained with the nozzle in place. Similar measurements have been taken with a solid end wall and are reported in Reference 1. A comparison between the reflected-shock test time with and without the nozzle presented in Figure 14 illustrates the amount of experimental scatter experienced. The mass flow through the nozzle was found to have no significant effect on the reflected-shock test time. It was also found by comparing the radiation-intensity measurements that the present nozzle throat had no influence on the uniformity of the reflected-shock gasdynamics.

5. NOZZLE BOUNDARY-LAYER GROWTH FOR RESERVOIR TEMPERATURE OF 7800°K AND PRESSURE OF 3.74 ATM.

Detailed measurements were made of the boundary-layer growth on the sidewall of the conical nozzle discussed in Section 2.1. Radial surveys of pitot pressure and stagnation-point heat-transfer rate were obtained at several axial stations as discussed in Section 2. Additionally, sidewall static pressure and temperature were measured as a function of axial distance from the throat. Typical results of the static-pressure measurements were reported in Figure 5.

Figure 15 is typical of the pitot-pressure records obtained in the nozzle. These particular results were obtained at an axial location 28-inches from the throat and illustrate the radial symmetry of the nozzle flow within $\pm$3 inches from centerline. The centerline pitot pressure reaches a plateau value within a period of time approximately equal to the nozzle starting time reported in Figure 9. The centerline pitot-pressure plateau remains for a period of approximately 200μsec. The pressure measurements obtained at $\pm$3 inches from centerline suggest that the flow at that location is not as uniform as it is on centerline. Some insight into the problem can be obtained by studying the radial pitot-pressure distribution presented in Figure 16, which illustrates the relatively good radial symmetry of the flow, and noting that the peak in the pitot-pressure distribution occurs near the $\pm$3 inch location. The presence of these peaks is thought to be due to the interaction between the boundary layer and the hypersonic flow as described by Poplawski,[32] among others. For the experimental conditions studied, the local Reynolds numbers are consistent with those assumed in the study by Poplawski. The pitot-pressure record obtained at 5 inches from centerline (note that this scope was triggered at a station different from the other records of this figure) appears to attain a plateau value in a somewhat shorter time than is required to reach a plateau value at the centerline. This result was generally observed at this experimental condition and is probably due to the substantially greater gas density near the wall (radial density profile will be shown later) than at the centerline.

Radial surveys of the stagnation-point heat-transfer rate were also obtained at several axial locations as described in Section 2. Figure 17 is typical of the radial profiles of heat-transfer rate. This result was obtained at an axial location of 31 inches. Figure 4 presents typical data records of the stagnation-point heat-transfer rate from which the profiles were deduced. The radial distribution suggests a relatively uniform core flow followed by an interaction region which is felt to be the result of the interaction between the boundary layer and the inviscid free stream.

5.1 Boundary-Layer Velocity and Density Profiles

The radial distribution of pitot-pressure and stagnation-point heat-transfer rate presented in Figures 16 and 17 can be used to deduce the radial velocity profile. If it is assumed that the continuum flow stagnation-point heat-transfer rate can be described by the relation[33]

$$\dot{q}_s = \frac{1}{\sqrt{R}} \; (0.614) \left(\frac{\rho}{\rho_{S.L.}}\right)^{0.5} \; \left(\frac{u}{10^3}\right)^{3.15} \tag{1}$$

and that the pitot pressure can be written as (ρ S.L. in Equation 1 is the sea-level density)

$$p_o' = \left[1 - \frac{1}{2} \left(\frac{\gamma - 1}{\gamma + 1}\right)\right] \; \frac{\rho u^2}{g_c} \tag{2}$$

Then if Equation 1 is divided by the square root of Equation 2 one obtains

$$\frac{\dot{q}_s}{\sqrt{p_o'}} = \frac{\sqrt{g_c} \; (0.614) \; (u)^{2.15}}{\sqrt{R} \left[1 - \frac{1}{2} \left(\frac{\gamma - 1}{\gamma + 1}\right)\right]^{0.5} (10^3)^{3.15}} \tag{3}$$

which, if the quantity $\left[1 - \frac{1}{2} \left(\frac{\gamma - 1}{\gamma + 1}\right)\right]^{0.5}$ is assumed to be radially constant, can be reduced to

$$\frac{u}{u_\ell} = \left[\frac{\dot{q}_s / \sqrt{p_o'}}{\left(\dot{q}_s / \sqrt{p_o'}\right)_\ell}\right]^{0.465} \tag{4}$$

Equation 4 was used in conjunction with the results presented in Figures 16 and 17 to deduce from the experimental data the velocity profile, (u/u_{ℓ}), presented in Figure 18. The resulting velocity profile indicates a relatively uniform velocity core followed by a significant velocity decrease consistent with the boundary-layer flow.

By combining Equations (2) and (4), one obtains a relation for the density distribution across the nozzle given by

$$\frac{\rho}{\rho_{\ell}} = \left[\frac{\rho_o'}{(\rho_o')_{\ell}}\right] \left[\frac{u_{\ell}}{u}\right]^2 \tag{5}$$

The radial density distribution was calculated from Equation (5) using the results presented in Figures 16 and 18. A typical radial density distribution is shown in Figure 19. For this particular experimental condition and location in the nozzle, the density increases very rapidly near the wall to a value that is approximately in order of magnitude greater than the centerline value. Since the sidewall static pressure and sidewall temperature were measured, it is relatively simple to relate the wall density to the centerline density if the molecular weight is assumed to be frozen at the reservoir value. This procedure was followed and the calculated wall-density ratio is compared to the deduced density distribution in Figure 19. Relatively good agreement is achieved between the calculated wall density and the value that would be obtained by extrapolating the radial distribution to the wall. Equally good agreement was obtained for each of the axial locations.

5.2 Comparison of Boundary-Layer Measurements with Theory

The displacement thickness, δ_*, for axially-symmetric nozzle flow can be calculated from the relation[34]

$$\delta_* - \frac{\delta_*^2}{2 r_w} = \delta \left[\int_0^1 \left(1 - \frac{\rho u}{\rho_e u_e}\right)\left(1 - \frac{y}{r_w}\right) d\left(\frac{y}{\delta}\right)\right] \tag{6}$$

The boundary-layer edge can be defined as that point at which the pitot pressure begins to decrease, and thus all of the quantities necessary for the calculation of the displacement thickness are available. It is important to note that the

fluid-flow parameters used in this calculation have been obtained from experimental measurements.

Figure 20 presents a comparison of the displacement thickness calculated from Equation (6) with the turbulent boundary-layer theory of Burke and Wallace[11] and the laminar boundary-layer correlation of Summers.[14] In the following paragraphs, a brief review of these theories is given.

Summers[14] obtained convenient correlations for boundary-layer growth and displacement-thickness growth based on experimental measurements obtained at AEDC. His correlation parameter is a function of reservoir temperature and pressure, cone angle, throat radius, and axial location in the nozzle. The reservoir pressures of the AEDC experiments were comparable to those experienced in the current work, but the corresponding reservoir temperatures were substantially lower. The relatively good correlation between the boundary-layer displacement thickness measured here and that predicted is interesting since little similarity exists between the two facilities in which the experimental data were obtained. Summers' data were obtained in the 18 inch LORHO wind tunnel at AEDC (arc driven) and the current data were obtained in a pressure shock tube, nozzle facility.

The Burke and Wallace[11] technique is somewhat more difficult to apply since a calculation of the inviscid-core gasdynamic variables is required. In their work, the boundary-layer thickness and displacement thickness are correlated as a function of a local Reynolds number computed using the Eckert[35] reference enthalpy method. Thus, from the calculation of the inviscid gasdynamics, a unit Reynolds number is calculated as a function of inviscid area ratio. After experimentally determining the displacement thickness at a given axial location, the appropriate inviscid area ratio is determined which must then be used to determine the Reynolds number used in their correlation. In order to apply the correlation of Reference 11 to the current experimental data it was necessary to extrapolate their results to lower Reynolds numbers.

A comparison between the experimentally determined boundary-layer thickness and the prediction of the two theories is also presented in Figure 20. The

experimental data points fall between the two predictions. In applying the correlation of Burke and Wallace to this experimental condition, it was necessary to separate the energy frozen in dissociation when computing the reference enthalpy. Neither of the boundary-layer prediction techniques compares as well with the experimental data as was shown for the displacement thickness.

5.3 Effective Inviscid Area Ratio

The inviscid area ratio at the various axial stations can be calculated from the deduced boundary-layer displacement thickness and the known nozzle geometry. The theoretical centerline pitot pressure can then be calculated (from Equation (2)) as a function of inviscid area ratio from the results of a numerical solution[36,37] of the quasi-one-dimensional, inviscid flow of reacting-gas mixtures. In this calculation, from an assumed equilibrium reservoir, the vibrational and electronic degrees of freedom are assumed to remain in thermal equilibrium with translation while the chemical reactions proceed at finite rates. The results of such a comparison are presented in Figure 21. The agreement between the experimental data and the theoretical prediction is excellent with the exception of the data point at the greatest inviscid area ratio (axial distance of 71 inches) from the throat. Lack of agreement at this location is not surprising since it is at this location that the quasi-one-dimensional approximation is expected to be least valid. An additional contribution to the lack of correlation is that difficulty was encountered in accurately resolving the pitot-pressure and stagnation-point heat-transfer profiles at this location because of the large boundary-layer thickness.

Figure 22 illustrates that for this particular experimental condition, the measured sidewall static pressure was significantly greater, at a given inviscid area ratio, than the theoretical value. The displacement-thickness results discussed above were used to determine the effective inviscid area ratio at which the theoretical and experimental static pressures are compared. The data presented in Figure 22 suggest the presence of a substantial normal pressure gradient. At this experimental condition, the boundary layer is very thick which may be a contributing factor to the discrepancy between measured and theoretical sidewall pressure.

6. NOZZLE BOUNDARY-LAYER GROWTH FOR RESERVOIR TEMPERATURE OF 6830°K AND PRESSURE OF 25 ATM.

As previously noted, detailed boundary-layer measurements were also obtained for a reflected-shock reservoir temperature of 6830°K and a pressure of 25 atm. The displacement thickness and effective inviscid area ratio for the expansion were deduced from the experimental pitot-pressure and stagnation-point heat-transfer rate data using the method also outlined in Section 3.6.

Figure 23 presents a typical radial pitot-pressure distribution obtained at an axial location 48 inches from the throat. The magnitude of the peak in the pitot-pressure distribution, which was discussed in Section 3.6, is significantly reduced from what it was in the previous experiments. In fact, the profiles taken at 28 and 38 inches did not illustrate a peak in the pitot pressure. These profiles were very uniform across the inviscid core followed by a rather sharp decrease in pressure. For this reservoir condition, the local Reynolds numbers at comparable nozzle locations are significantly greater than they were at the previous experimental condition. Further, the experimentally determined boundary-layer thicknesses at comparable axial stations were significantly smaller for this, a higher reservoir pressure condition.

The stagnation-point heat-transfer rate profile corresponding to the pitot-pressure profile discussed above is shown in Figure 24. A relatively uniform inviscid core is suggested by the measurements, followed by a rapid reduction in heat-transfer rate within the boundary layer.

6.1 Boundary-Layer Velocity and Density Profiles

Figures 23 and 24 were used to obtain the velocity profile across the nozzle radius presented in Figure 25. This velocity profile, which is characteristic of those obtained at the remaining stations, is significantly more full than profiles at the lower pressure experimental condition.

The radial-density distribution determined from the experimental data is shown in Figure 26. The calculated density ratio at the wall is once again in

reasonable agreement with an extrapolation of the radial profile. The density gradient near the wall is substantially less than it was for the previous experimental condition. This is not unexpected, since the free-stream density is also greater than previously and, in addition, the boundary layer is substantially thinner.

6.2 Comparison of Boundary-Layer Measurements with Theory

By utilizing the results presented in Figures 25 and 26, the local boundary-layer displacement thickness and inviscid area ratio were calculated. The experimentally determined pitot pressure is compared with the theoretical quasi-one-dimensional calculation in Figure 27. Once again, the agreement between theory and experiment is good, with the exception of the data point at the largest area ratio (71 inches from the throat). In this case, however, the experimental data point at this station falls below the theory whereas, in the previous case (see Figure 21), it was above the theory. Once again, the validity of the one-dimensional-flow approximation is somewhat doubtful at this location.

For comparison purposes, the experimentally determined displacement thickness and boundary-layer thickness are compared with the correlations of Burke and Wallace[11] and Summers[14] in Figure 28. For this particular experimental condition, the results of the two correlations are very nearly equal to each other. Further, the experimental data are in good agreement with the two predictions. Thus, it appears that either of the correlations predicts the experimental data within the accuracy of the comparison.

In contrast to the previous experimental condition, the measured sidewall static pressure was in good agreement with the theoretical value (from the one-dimensional calculation previously discussed) at the corresponding inviscid area ratio. Figure 29 illustrates this agreement and suggests the absence of any pressure gradient normal to the wall in these experiments.

7. EQUILIBRIUM-INTERFACE STUDIES

Experiments were conducted in the shock tube and in the nozzle at incident-shock Mach numbers ranging from 7.3 to 12.2 in order to determine the range of validity of the equilibrium-interface concept for shock-tunnel operation and are reported in detail in Reference 21. The potential advantage of this technique of shock-tube operation is the significant gain in reflected-shock enthalpy that might be achieved. For this reason, the results of Reference 21 are pertinent to the material reported here and a brief summary is given here. Copper[23] used reflected-shock pressure measurements and the equilibrium interface concept to conclude that for his experiment at an incident-shock Mach number of 7.26, an equilibrium enthalpy could be realized that was approximately 1.5 times the enthalpy associated with the gas immediately after shock reflection. On the basis of the pressure data alone similar gains appear to have been achieved for both hydrogen and helium drivers in the present experiments. However, the accompanying radiation-intensity data show that the pressure data may be misleading and that higher enthalpy levels may not have been achieved except possibly in the case of the helium driver. Copper used a helium driver but obtained no radiation-intensity data. It is not possible to use the present data to support or disprove Copper's conclusion. In the following paragraphs the experiments conducted in the shock tube and in the nozzle in order to assess the validity of the equilibrium interface concept are discussed.

7.1 Shock-Tube Experiments

Conditions in the reflected-shock reservoir were investigated prior to the study of fluid-flow characteristics of the nozzle flow. To this end, the radiation-intensity and pressure characteristics of the reflected-shock processed gas were studied over the entire range of incident-shock Mach numbers of interest. Data were recorded (several milliseconds) after shock reflection.

Figure 30 illustrates the sidewall and end-wall radiation-intensity and the end-wall pressure records obtained at the lowest incident-shock Mach number of interest for the case of hydrogen driving air. The magnitude of the initial pressure plateau shown in Fig. 30 (a) was always within a few percent of the theoretical value of Feldman[26]. At this shock Mach number the character of the reflected-shock radiation-intensity obtained at 3/4-inch from the end wall is

very similar to the end-wall pressure record as can be seen by comparing Figures 30 (a), (b) and (c). This similarity between the pressure and radiation-intensities shown in Figure 30 was only observed over a narrow range of incident shock Mach numbers (7.3 to 8.5). The end-wall radiation-intensity record presented in Figure 30 (d) illustrates the characteristic linear rise after shock reflection from the end wall which is consistent with an optically thin gas and a reflected shock moving at a constant velocity away from the end wall. The linear rise occurs with only slight irregularities for the entire duration of the recording period. In subsequent data records presented here for higher incident-shock Mach numbers the linear rise of the end-wall radiation-intensity is terminated by a sharp decrease after approximately 200-400 μsec. Also illustrated in Figure 30 (a) is the "pressure-dip" which, for this experimental condition occurs at approximately 650 μsec after shock reflection. A wave diagram discussed later indicates that the dip is associated with reflection of an expansion wave from the driver-driven gas interface even though for these operating conditions the interface should have been near tailored.

At incident-shock Mach numbers greater than 8.5 the character of the radiation-intensity history is no longer qualitatively similar to the end-wall pressure when hydrogen is used as the driver gas. Specifically, a pressure increase with a correspondingly greater enthalpy level (if the compression were isentropic) was not accompanied by a corresponding increase in radiation-intensity. This non-similarity became increasingly greater as the incident-shock Mach number was increased and is illustrated in Figure 31 which presents the end-wall pressure and radiation-intensity measurements for an incident shock Mach number of 12.2. At this condition, it becomes obvious that at times greater than 200 μsec after shock reflection, the radiation-intensity time history differs greatly from the end-wall pressure time history. It appears that after 450 μsec the gas temperature cannot be calculated from the pressure record as would be the case if the equilibrium-interface concept were valid. As the pressure begins to increase at 450 μsec towards a second plateau the radiation-intensity actually begins to decrease from a level that is already less than that corresponding to the plateau immediately after shock reflection. These studies indicate that for a hydrogen driver gas, at least, the equilibrium interface concept offers little potential for achieving higher enthalpy levels than can be obtained from conventional operation.

Figure 32 is typical of the results obtained for helium driving air. For this particular experimental condition the forementioned "pressure-dip" is present suggesting an under-tailored interface. Again, the initial end-wall pressure plateau corresponds very nearly to the theoretical reflected shock pressure. The most significant difference between the helium and hydrogen experiments is that the reflected-shock radiation intensity appears to follow the end-wall pressure if helium is used as the driver gas. On the basis of these data, it is still not completely certain that the high-temperature gas is chemically pure at times beyond the initial radiation-intensity plateau. In contrast to the hydrogen results there is no indication to the contrary, that is, that the high-temperature gas has been diluted by cold gas. However, the line reversal measurements of Lapworth and Townsend[38] provide sufficient reason to be doubtful of the validity of the equilibrium-interface concept even when helium is used to drive nitrogen. This marked effect of driver gas on the behavior of the measurements of the reflected-shock processed gasdynamics was observed in all cases where comparisons at equivalent incident shock Mach numbers were made. It is important to note that the enthalpy level achieved in the equilibrium interface region in the case of the helium driver operated at the highest allowable pressure in this facility was significantly less than that achieved immediately behind the reflected shock using a hydrogen driver at the same driver pressure at an appropriately higher Mach number.

Several experiments were conducted in an effort to obtain some insight into the cause of the "pressure-dip" referred to earlier. In the first of these, helium instead of hydrogen was used to drive air (see Fig. 32). Comparison of results obtained at comparable Mach numbers indicated that the helium does not eliminate the dip but it does reduce its magnitude by a factor of approximately 1.5.

The driven-tube gas was also varied and Figure 33 presents results obtained for hydrogen driving nitrogen. However, for this particular shock-tube condition, the "pressure-dip" is not observed in the end-wall pressure data. The general features of the radiation-intensity and end-wall pressure data are consistent with the air experiments. The dip does not completely disappear when using nitrogen since subsequent experiments were conducted at increased incident-shock Mach numbers and the "pressure-dip" was observed. The magnitude of this dip

was comparable to that measured in the case of helium driving air. The results of the experiments discussed in this section suggest that it is the character of the interface that is responsible for the "pressure-dip" and the limited application of the equilibrium-interface concept. It is well known that the interface is not ideal and that finite gradients of density and temperature can exist.

A simple wave diagram shown in Fig. 34 was constructed from the experimental results of Fig. 31 which were obtained for hydrogen driving air. The letters adjacent to the data points of Fig. 34 are also given on Fig. 31 for reference purposes. The solid lines on Fig. 34 have been faired through the data. Data points a, g, and h were obtained from the end-wall pressure data where as the remaining data were determined from the radiation-intensity data. Point d was obtained from the end-wall radiation-intensity measurement by assuming that the reflected shock moved away from the end wall at theoretical velocity[26] and calculating the distance the shock would have moved in the time elapsed between points a and d (see Fig. 31 (e)). The velocity of the wave d-e-f-g is within 10 percent of the calculated sonic velocity in the reflected-shock processed gas. All of the diagnostics are consistent in suggesting the presence of the expansion region shown on Fig. 34. The presence of such an expansion at this Mach number is of course inconsistent with a real gas wave diagram calculation which would have predicted d-e-f-g to be a shock wave. Such an expansion would be possible if the interface gas, composed primarily of hydrogen, were locally heated, thus drastically altering the local speed of sound. The energy necessary for heating could come from several sources, among them being energy liberated from hydrogen-oxygen combustion[39,40]. However, on the basis of the results presented it is obvious that the "pressure-dip" cannot be completely explained by the interface combustion postulate since it was also observed, but of lesser magnitude, when nitrogen was driven by hydrogen and when air was driven by helium. It is thus suggested that temperature or density gradients existing in the interface region cause the dip and that interface combustion significantly amplifies its magnitude.

7.2 Nozzle Experiments

All of the results presented in Section 7.1 were obtained with a solid shock-tube end wall, i.e., with no flow into the nozzle. The nozzle was subsequently installed and the results presented in this section were obtained.

Figure 35 presents typical nozzle measurements for an incident-shock Mach number of 9.9. It is interesting to observe that the nozzle radiation-intensity, microwave-interferometer and Langmuir-probe measurements all show similar features. The microwave interferometer and the photomultiplier tube both give the same values for the duration of uniform flow at 21.5 inches from the throat. The duration of uniform nozzle flow at the various locations is of the same magnitude as the duration of uniform reflected-shock radiation-intensity immediately after shock reflection. It was generally concluded that a close similarity exists between the early time history of the reflected-shock radiation intensity obtained 3/4-inch from the end wall and the time history of the radiation-intensity, microwave interferometer and Langmuir-probe measurements made in the nozzle. The electron density and radiation-intensity data presented in Figure 35 illustrate that the period of uniform nozzle flow is followed by an increase and subsequent decrease in both of these quantities. However, there does not appear to be a significant period of uniform electron density or radiation intensity corresponding to the elevated temperature and pressure of the equilibrium-interface region.

Nozzle measurements were also obtained for hydrogen driving nitrogen and are presented in Figure 36. The most significant difference between the microwave-interferometer, Langmuir-probe and radiation-intensity data presented in Figures 35 and 36 is the magnitude of the signal terminating the uniform flow. The early-time character of the radiation-intensity records is similar. The characteristics of the constant bias voltage Langmuir-probe records are also similar except that the magnitude of the signal terminating the uniform-flow period is substantially greater for the air experiments. The basic difference in the two microwave-interferometer data records also occurs after termination of the uniform nozzle-flow period. The late-time phase-shift data of Figure 36(d) suggests a very rapidly changing plasma. Note that the general

characteristics of the Langmuir-probe and radiation-intensity data records shown in Figure 36(c) and (e) are similar to the reflected-shock radiation-intensity data presented in the upper trace of Figure 36(a).

The characteristics of the radiation-intensity and electron-density records after termination of the uniform-flow period were not always reproducible as previously noted in Section 4.1. By contrast, the early-time histories including that period defined as duration of uniform flow were very reproducible. The composite results were consistent in suggesting that one should be very careful in applying the equilibrium-interface concept to nozzle flows if hydrogen is used as the driver-tube gas. For the hydrogen driver, no significant period of uniform nozzle flow associated with the equilibrium-interface region could be found. This is consistent with the result obtained in the reflected-shock reservoir. Corresponding detailed nozzle measurements at comparable Mach numbers could not be obtained for the helium driver because of facility limitations. However, the results presented for the shock tube only suggested that the equilibrium interface concept may have been valid under some conditions for this driver gas.

8. CONCLUSIONS

A detailed experimental study of the starting process and boundary-layer growth in high-enthalpy, low-density nozzle flows has been described. Two experimental conditions were studied. In the first, the incident-shock Mach number was 16.50. The corresponding reflected-shock pressure and temperature were 3.74 atm. and 7800°K, respectively. The incident-shock Mach number at the second condition was 11.6. The corresponding reflected-shock pressure and temperature were 25 atm. and 6830°K, respectively.

The time required to establish uniform flow at various axial locations in the nozzle has been measured experimentally using several diagnostic techniques. This time was found to increase approximately linearly with axial distance from the nozzle throat. The results indicated that the pitot-pressure, Langmuir-probe, microwave-interferometer, radiation-intensity, sidewall pressure, and stagnation-point heat-transfer rate measurements are all effective for determining the time required to establish uniform nozzle flow. It is further suggested that at the initial nozzle pressures used the starting process is dominated by an expansion fan and that disturbances prior to the expansion fan consume only a small portion of the total starting time.

The duration of uniform flow at various axial locations was also measured using the diagnostic techniques noted in the preceding paragraph. Radiation-intensity, Langmuir-probe and microwave-interferometer measurements, which are considered to be the best indicators of uniform flow, indicated time durations significantly less than that deduced from the pitot-pressure measurements. Stagnation-point heat-transfer rate measurements were found to be of little value in determining the duration of uniform nozzle flow.

The experimentally determined velocity and density profiles were used to obtain the boundary-layer displacement thickness growth and corresponding effective inviscid area ratios. For both experimental conditions, the measured pitot pressures were then compared to the results of a quasi-one-dimensional nonequilibrium-expansion calculation and found to be in good agreement. It was thus concluded that, for a significant portion of the nozzle, the one-dimensional

flow approximation was reasonably valid. Comparison between the measured and theoretical sidewall static pressure suggested that for the low-reservoir-pressure experiment a significant normal pressure gradient was present. At the higher reservoir pressure the measured and theoretical sidewall static pressures were in excellent agreement. In the case of the higher reservoir-pressure experiment, good agreement was found between the present experimentally determined boundary layer and displacement-thickness growth and the results of the Burke and Wallace[11] prediction technique. For the low reservoir-pressure experiment, the boundary-layer displacement thickness was in good agreement with the prediction of Summers,[14] but the boundary-layer thickness was not.

The equilibrium-interface concept as applied to shock tube and shock-tunnel flows was studied for Mach numbers ranging from 7.3 to 12.2. The duration of uniform reflected-shock conditions was found to be confined to a period of time immediately following shock reflection. The duration of uniform flow at various nozzle locations was in general less than the duration of this initial reflected-shock condition. When hydrogen was used as the driver-tube gas, the Mach number range over which the equilibrium interface concept appeared to be valid was very limited. Use of helium as the driver gas resulted in a significant difference in the character of the reflected-shock radiation intensity, which suggested the possible validity of the concept. However, it was not feasible to make detailed measurements in the nozzle because of the low signal levels.

The cause of the dip frequently observed in the reflected-shock end-wall pressure was also investigated in some detail. The results suggest that the dip is caused by the imperfect nature of the interface and amplified by the presence of combustion. Both nitrogen and air were used as driven-tube gas and either hydrogen or helium was used as the driver gas. The "pressure-dip" was found to be present to some degree for all combinations of driver and driven tube gas. The magnitude of the dip was greatest when hot hydrogen was used to drive air. A wave diagram constructed from the experimental data suggested that the dip was the result of an expansion fan that is reflected when the reflected shock interacts with this driver-driven gas interfacd.

REFERENCES

1. Dunn, M.G., "Experimental Shock-Tube Investigation of Conditions Behind Incident and Reflected Shocks in Air for Shock Mach Numbers Between 8.5 and 16.5, "Fifth Hypervelocity Techniques Symposium, Vol. 1, University of Denver (March 1967).

2. Bull, G.V., "Starting Processes in an Intermittent Wind Tunnel," University of Toronto, Inst. of Aerospace Report No. 12 (February 1951).

3. Parks, E.K., "Supersonic Flow in a Shock Tube of Divergent Cross-Section," University of Toronto, Inst. of Aerospace Report No. 18 (May 1952).

4. Glick, H.S., Hertzberg, A., Smith, W.E., "Flow Phenomena in Starting a Hypersonic Shock Tunnel," Cornell Aeronautical Laboratory, Report No. AD-789-A-3 (also AEDC-TN-55-16) (March 1955).

5. Henshall, B.D. and Gadd, G.E., "Factors Affecting the Performance of the Nozzle of a Hypersonic Shock Tube," ARC Rept. No. 18, 201 also CP 293 (February 4, 1956).

6. Holder, D.W., and Schultz, D.L., "The Duration and Properties of the Flow in a Hypersonic Shock Tunnel," American Rocket Society, Paper No. 1970-61, International Hypersonics Conference (August 16-18, 1961).

7. Smith, C.E., "An Analytic Study of the Starting Process in a Hypersonic Nozzle," Stanford U. Report SUDAER No. 135 (September 1962) (also see Proc. 1964 Heat Transfer and Fluid Mechanics Institute, Stanford U. Press).

8. Smith, C.E., "The Starting Process in a Hypersonic Nozzle," University of Oxford, Report No. 1000 (July 1965).

9. Ackroyd, J.A.D., "A Study of Running Times in Reflected Shock Tunnels," Aeronautical Research Council, Report 26, 631 Hyp 476 (January 1965).

10. Burke, A.F. and Bird, K.D., "The Use of Conical and Contoured Expansion Nozzles in Hypervelocity Facilities," Cornell Aeronautical Laboratory, Report No. 112 (July 1962).

11. Burke, A.F. and Wallace, J.E., "Aerothermodynamic Consequences of Nozzle Nonequilibrium," Arnold Engineering Development Center, AEDC-TR-66-47 (February 1966).

12. Cohen, C.B. and Reshotko, E., "The Compressible Laminar Boundary Layer with Heat Transfer and Arbitrary Pressure Gradient," NACA Report 1294 (1956).

13. Durand, J.A. and Potter, J.L., "Calculation of Thicknesses of Laminar Boundary Layers in Axisymmetric Nozzles with Low Density, Hypervelocity Flows," AEDC-TN-61-146 (December 1961).

14. Summers, W.E., "Real-Gas Laminar Boundary Layers in Hypervelocity Nozzles," AEDC-TR-65-217 (October 1965).

15. Wallace, J.E., "Hypersonic Turbulent Boundary Layer Studies at Cold Wall Conditions," 1967 Heat Transfer and Fluid Mechanics Institute, San Diego, California (June 19-21, 1967).

16. Burke, A.F., "Turbulent Boundary Layers on Highly Cooled Surfaces at High Mach Numbers," Cornell Aeronautical Laboratory, Report 118 (November 1961).

17. Johnson, A.F., "A Method of Calculating Boundary-Layer Thickness in Axisymmetric Nozzles with Laminar Hypersonic Flow," Sandia Corp., Report SC-4370 (October 1959).

18. Sivells, J.C. and Payne, R.G., "A Method of Calculating Turbulent Boundary-Layer Growth at Hypersonic Mach Numbers," AEDC-TR-59-3 (March 1959).

19. Levinsky, E.S. and Brainerd, J.J., "Inviscid and Viscous Hypersonic Nozzle Flow with Finite Rate Chemical Reactions," AEDC-TDR-63-18 (January 1963).

20. Wood, N.B., "Calculation of the Turbulent Boundary Layers in the Nozzle of an Intermittent Axisymmetric Hypersonic Wind Tunnel," Aeronautical Research Council (G.B.), C.P. No. 721 (September 1963).

21. Dunn, M.G., "Experimental Study of Reflected-Shock Tunnel Flows in the Equilibrium Interface Region, Cornell Aeronautical Laboratory, Report AM-1702-A-1 (January 1968).

22. Hertzberg, A., Smith, W.E., Glick, H.S., and Squire, W., "Modification of the Shock Tube for the Generation of Hypersonic Flow," Cornell Aeronautical Laboratory, Report AD-789-A-2 (March 1955).

23. Copper, J.A., "Experimental Investigation of the Equilibrium Interface Technique," Phys. of Fluids, Vol. 5, No. 7, pp. 844-849 (July 1962).

24. Copper, J.A., Miller, H.R., and Hameetman, F.J., "Correlation of Uncontaminated Test Durations in Shock Tunnels," Fourth Hypervelocity Techniques Symposium, Univ. of Denver, pp. 274-310 (Nov. 1965).

25. Skinner, G.T., "Analog Network to Convert Surface Temperature to Heat Flux," Cornell Aeronautical Laboratory, Report CAL-100 (February 1960).

26. Feldman, S., "Hypersonic Gas Dynamic Charts for Equilibrium Air," AVCO Everett Research Report 40 (January 1957).

27. Mirels, H., "Test Time in Low-Pressure Shock Tubes," Phys. Fluids, Vol. 6, No. 9, pp. 1201-1214 (September 1963).

28. Mirels, H., "Shock Tube Test Time Limitations Due to Turbulent-Wall Boundary Layer," AIAA Journal, Vol. 2, No. 1, pp. 84-92 (January 1964).

29. Mark, H., "The Interaction of a Reflected Shock Wave with the Boundary Layer in a Shock Tube," NACA TM 1418 (March 1958).

30. Friedman, M.P., "A Simplified Analysis of Spherical and Cylindrical Blast Waves," J. Fluid Mech. Vol. II, pp. 1-15 (1961).

31. Hall, J.G., "The Design and Performance of a 9-Inch Plate Mach-Zehnder Interferometer," Univ. of Toronto, Inst. of Aerospace Rept. No. 27 (March 1954).

32. Poplawski, B., Interaction Between the Boundary Layer and the Hypersonic Flow in a Conical Nozzle, ATD Report 66-54 (16 May 1966).

33. Detra, R.W. and Hidalgo, H., Generalized Heat Transfer Formulae and Graphs, AVCO Everett Research Report 72 (March 1960).

34. Wallace, J.E., Hypersonic Turbulent Boundary Layer Studies at Cold Wall Conditions, 1967 Heat Transfer and Fluid Mechanics Institute (February 1967).

35. Eckert, E.R.G., Engineering Relations for Friction and Heat Transfer to Surfaces in High Velocity Flow, Journal of the Aeronautical Sciences, pp. 585-587 (August 1955).

36. Eschenroeder, A.Q., Boyer, D.W. and Hall, J.G., Nonequilibrium Expansions of Air with Coupled Chemical Reactions, Phys. Fluids, Vol. 5, p. 615 (1962).

37. Lordi, J.A., Mates, R.E. and Moselle, J., Computer Program for the Numerical Solution of Nonequilibrium Expansions of Reacting Gas Mixtures, Cornell Aeronautical Laboratory Report AD-1689-A-6 (June 1965).

38. Lapworth, K.C. and Townsend, J.E.G., Temperature and Pressure Studies in the Reservoir of a Reflected-Shock Hypersonic Tunnel, ARC Rept. R and M 3479 (Dec. 1964).

39. Copper, J.A., Effects of Interface Combustion and Mixing on Shock-Tunnel Conditions, AIAA Journal, pp. 1669-1671, (September 1964).

40. Flagg, R.F., "Advances in Shock Tunnel Driving Techniques, Proc. of Third Hypervelocity Techniques Symposium, pp. 89-115, Denver Research Inst. (1964).

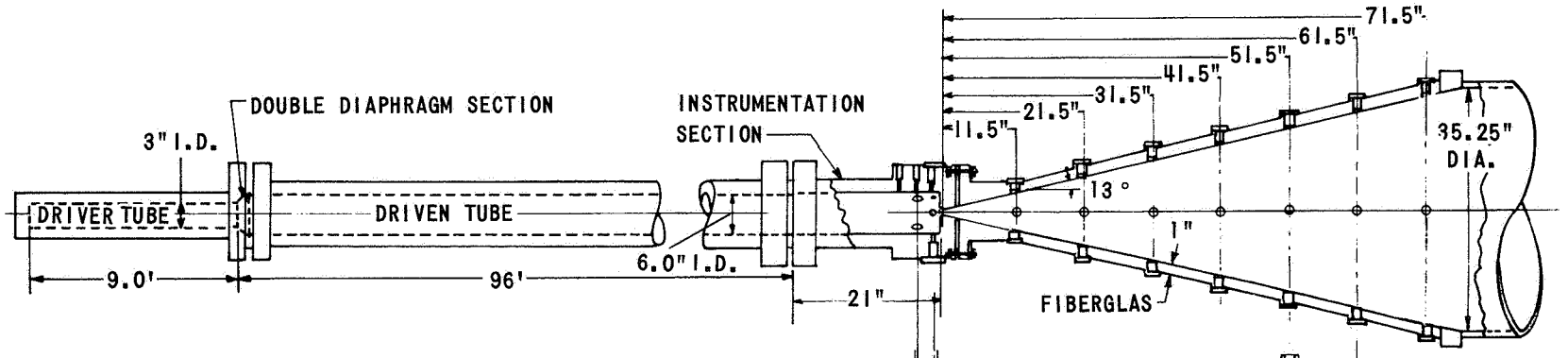

X	D
+ 1.25	1.144
+ 0.600	0.904
+ 0.300	0.820
0	0.748
- 0.300	0.696
- 0.600	0.656
- 1.200	0.608
- 1.500	0.591
- 2.000	3/16" RAD.

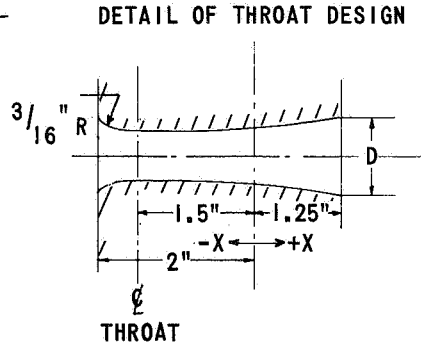

Figure 1 SCHEMATIC OF EXPERIMENTAL APPARATUS

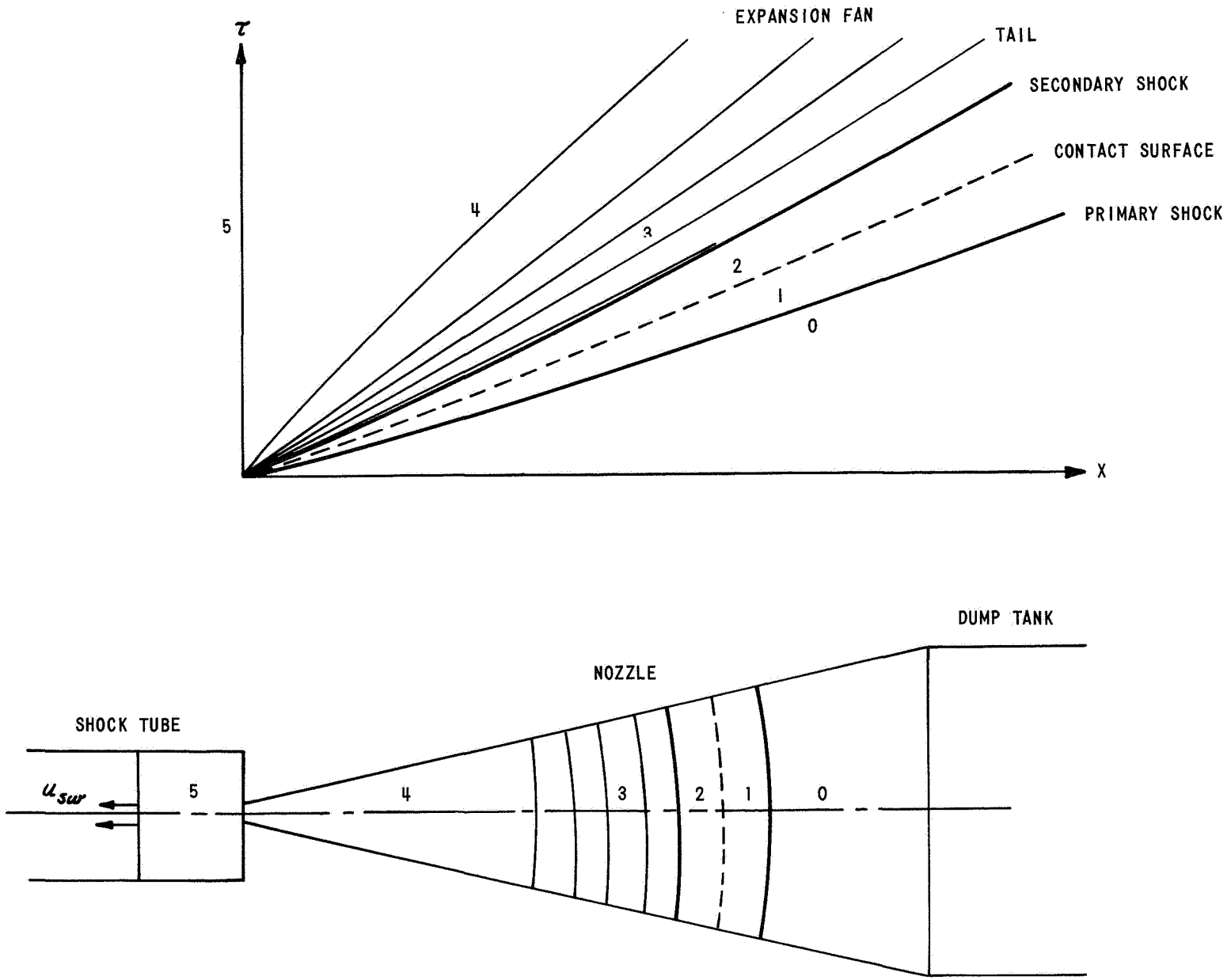

Figure 2 SKETCH OF POSSIBLE STARTING PROCESS IN NOZZLE

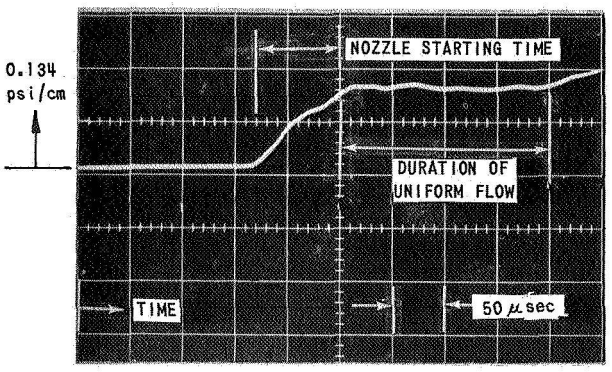

(a) CENTERLINE PITOT PRESSURE AT 28-INCHES FROM NOZZLE THROAT

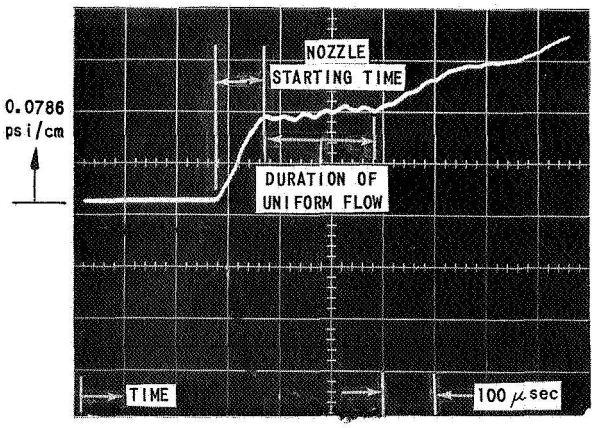

(b) CENTERLINE PITOT PRESSURE AT 38-INCHES FROM NOZZLE THROAT

DRIVER: 15,000 psi H_2 (760°F)
DRIVEN: 0.5 mmHg AIR
END-WALL MACH NO.: 16.5

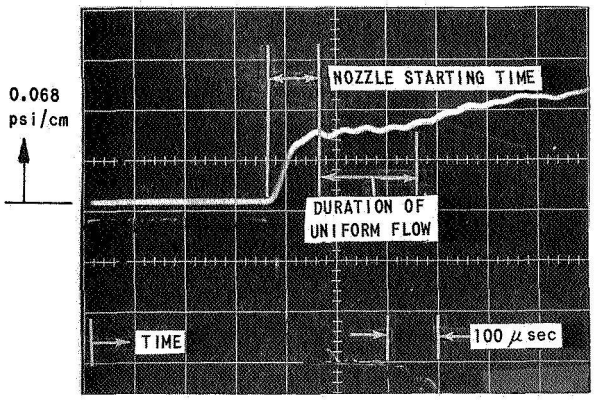

(c) CENTERLINE PITOT PRESSURE AT 48-INCHES FROM NOZZLE THROAT

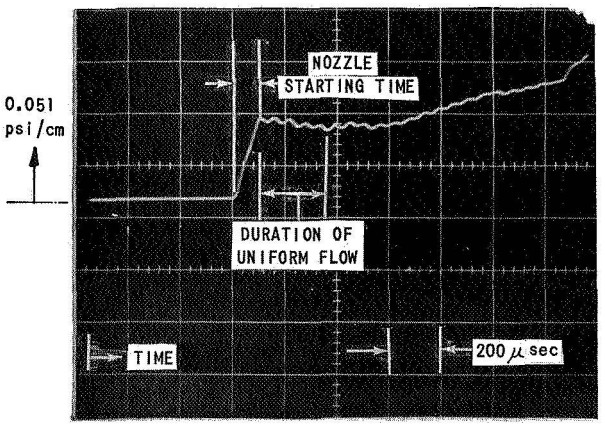

(d) CENTERLINE PITOT PRESSURE AT 68-INCHES FROM NOZZLE THROAT

Figure 3 PITOT-PRESSURE MEASUREMENTS ON CENTERLINE OF NOZZLE

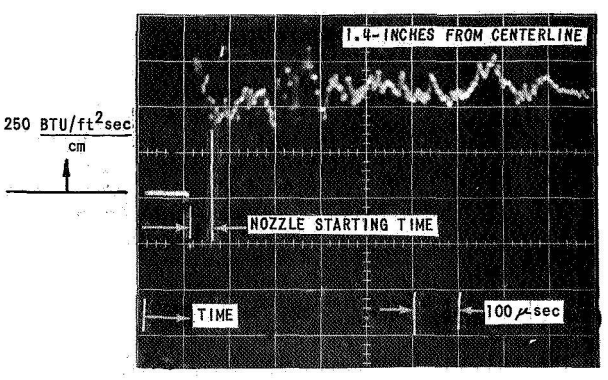

(a) HEAT-TRANSFER RATE AT 11-INCHES FROM NOZZLE THROAT

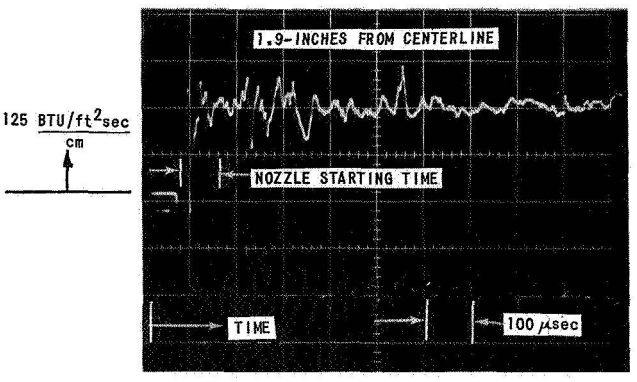

(b) HEAT-TRANSFER RATE AT 21-INCHES FROM NOZZLE THROAT

DRIVER: 15,000 psi H_2 (760°F)
DRIVEN: 0.5 mmHg AIR
END-WALL MACH NO.: 16.5

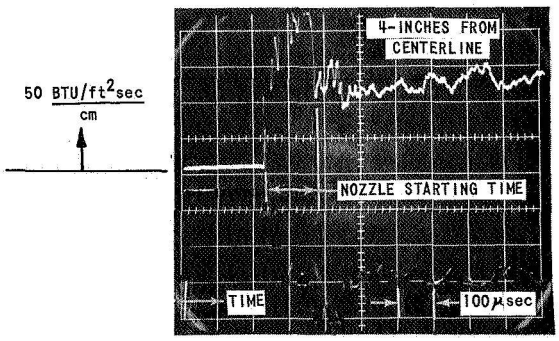

(c) HEAT-TRANSFER RATE AT 41-INCHES FROM NOZZLE THROAT

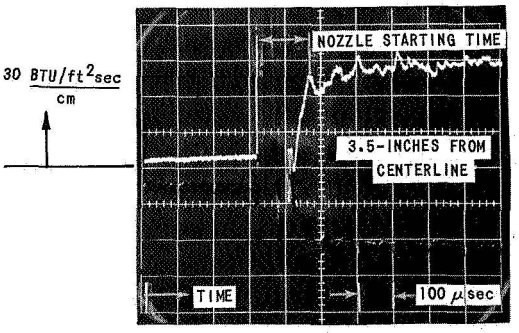

(d) HEAT-TRANSFER RATE AT 51-INCHES FROM NOZZLE THROAT

Figure 4 STAGNATION-POINT HEAT-TRANSFER RATE AT VARIOUS AXIAL LOCATIONS IN NOZZLE

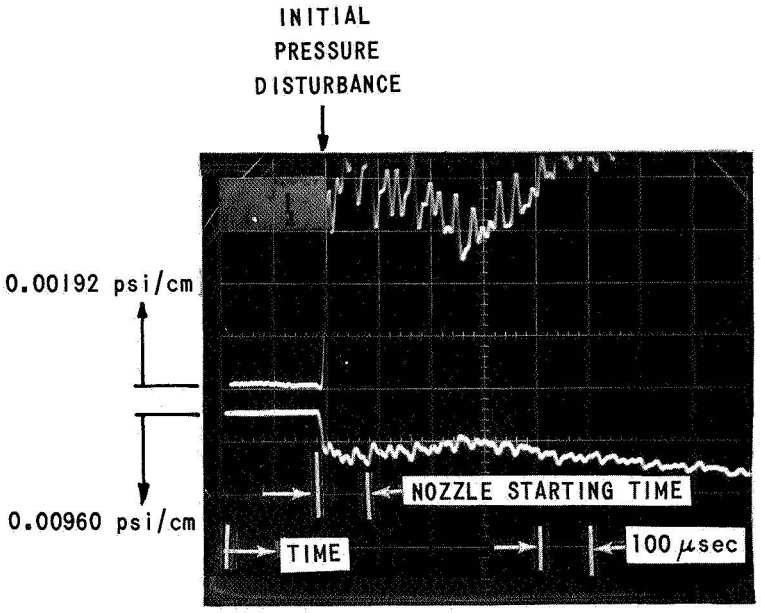

DRIVER: 15,000 psi H_2 (760 °F)
DRIVEN: 0.5 mmHg AIR
END-WALL MACH NO.: 16.5
AXIAL DISTANCE FROM THROAT: 21.5-inches

Figure 5 SIDEWALL STATIC-PRESSURE MEASUREMENT IN NOZZLE

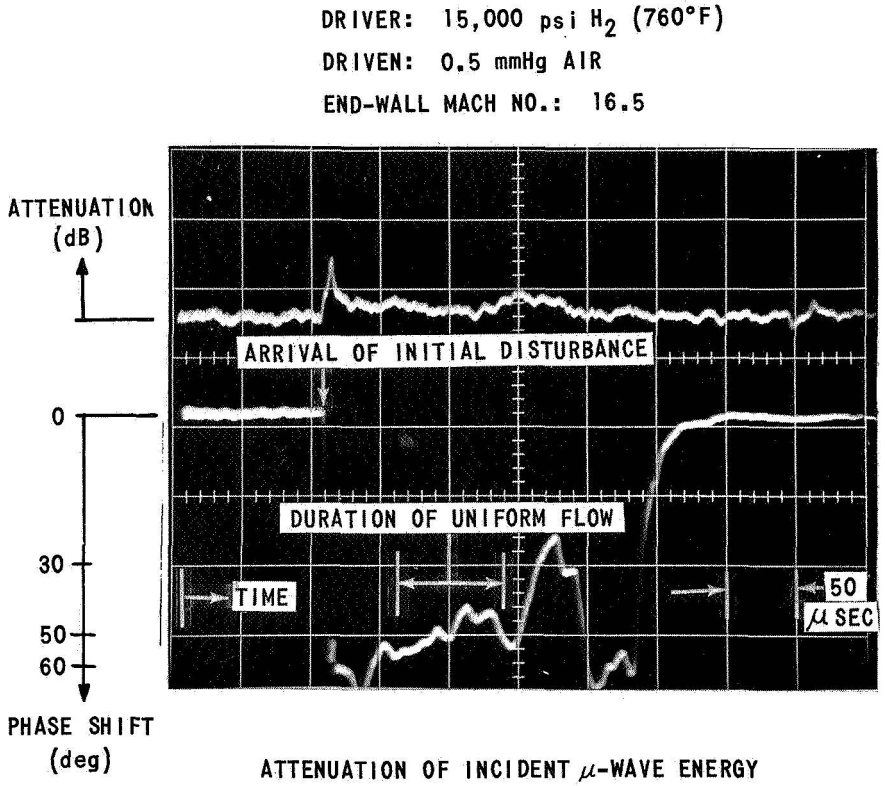

Figure 6 142 GHz MICROWAVE INTERFEROMETER DATA AT 11.5-INCHES FROM NOZZLE THROAT

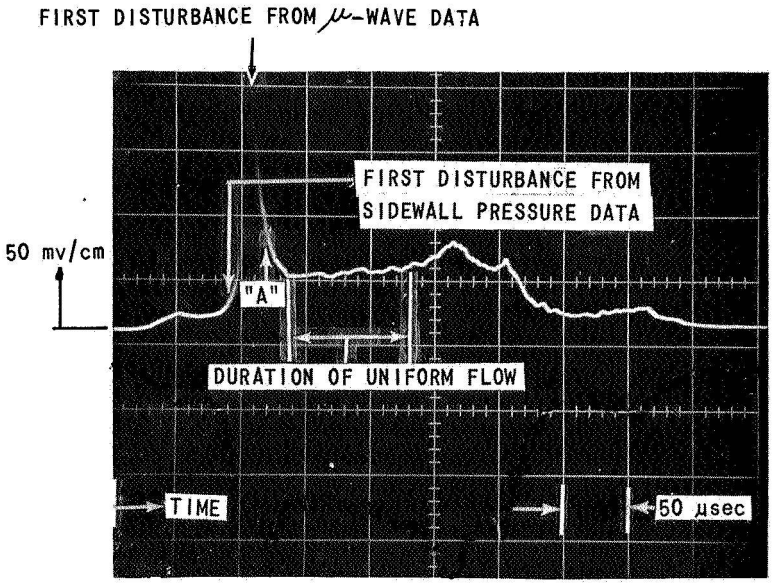

(a) RADIATION INTENSITY AT 11.5 INCHES FROM NOZZLE THROAT

DRIVER: 15,000 psi H_2 (760°F)
DRIVEN: 0.5 mmHg AIR
END-WALL MACH NO.: 16.5

NOTE: "A" DENOTES INITIATION OF UNIFORM FLOW FROM INTEGRATION OF (u-a)

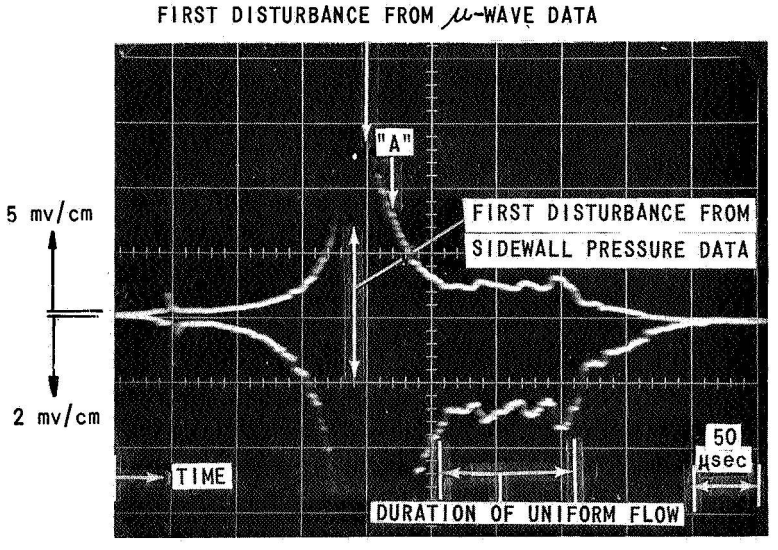

(b) RADIATION INSTENSITY AT 21.5 INCHES FROM NOZZLE THROAT

Figure 7 RADIATION-INTENSITY MEASUREMENTS NORMAL TO NOZZLE AXIS

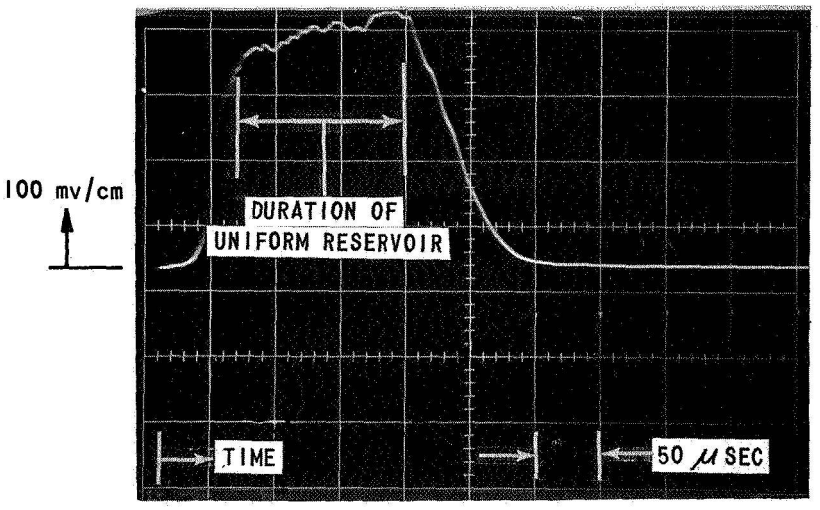

RADIATION INTENSITY $\frac{3}{4}$-INCH FROM END WALL

DRIVER: 15,000 psi H_2 (760°F)

DRIVEN: 0.5 mmHg AIR

END-WALL MACH NO.: 16.5

Figure 8 RADIATION INTENSITY NORMAL TO SHOCK-TUBE AXIS IN REFLECTED-SHOCK RESERVOIR WITH NOZZLE

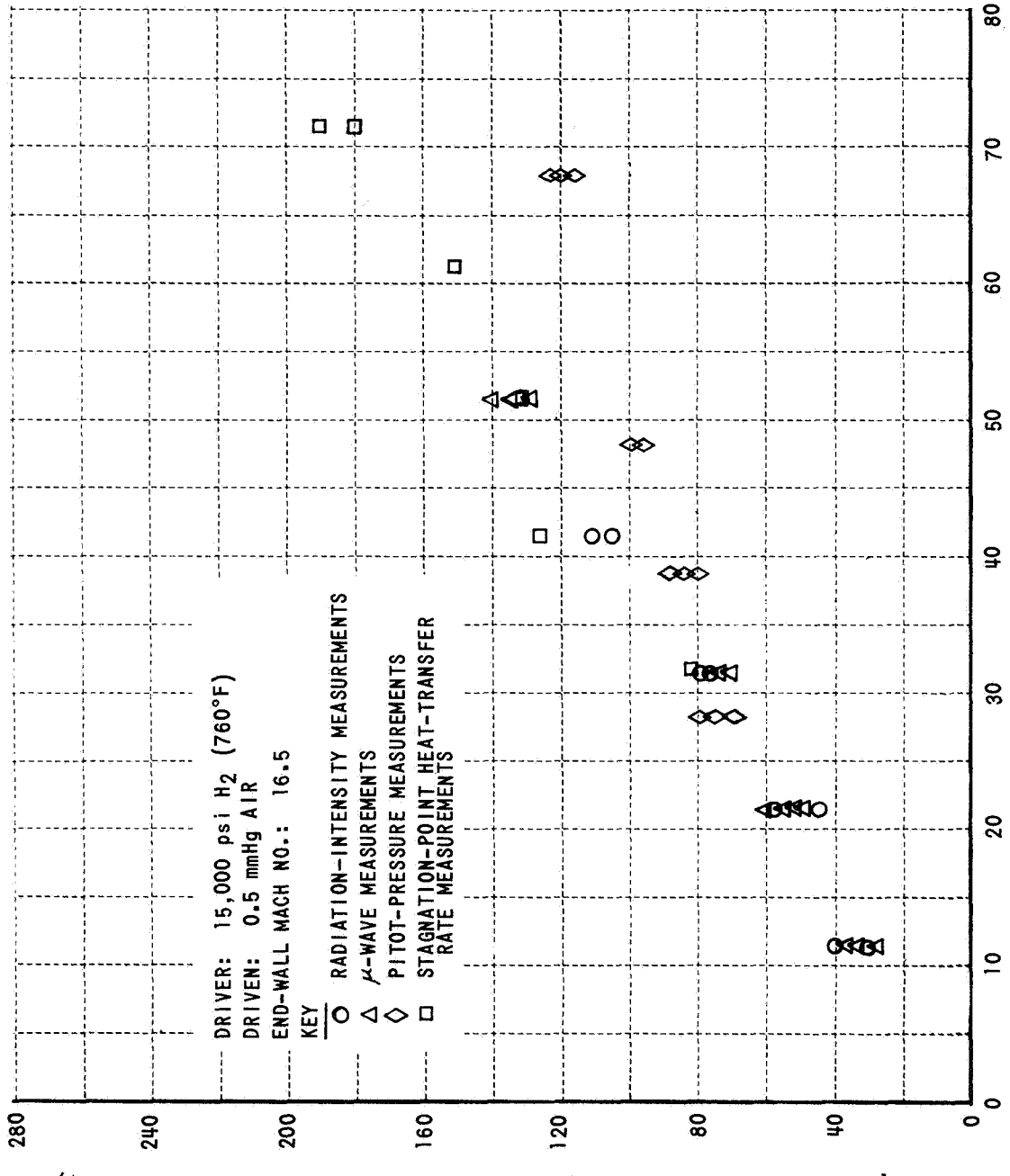

Figure 9 EXPERIMENTALLY DETERMINED NOZZLE STARTING TIME

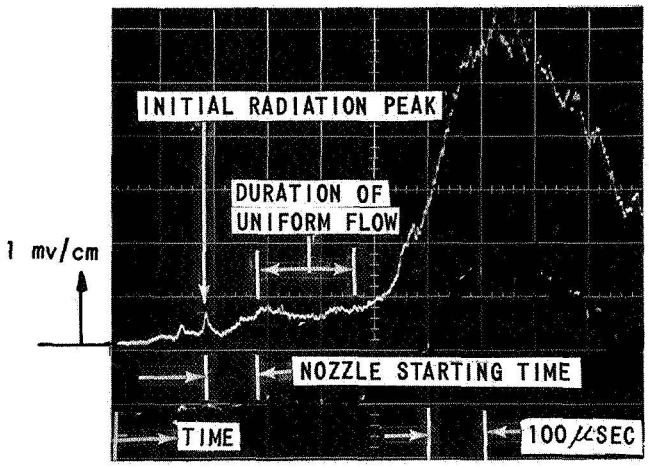

(a) RADIATION INTENSITY FOR INITIAL NOZZLE PRESSURE OF 2 MICRONS

DRIVER: 4000 psi H_2 (760°F)
DRIVEN: 10.0 mmHg AIR
END-WALL MACH NO.: 10.0
AXIAL DISTANCE FROM THROAT: 21.5 INCHES

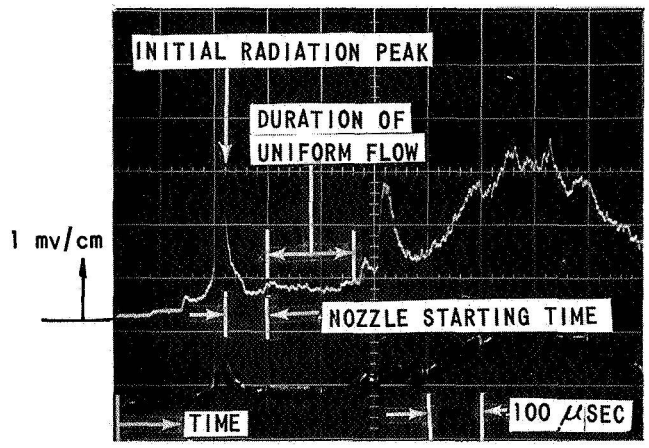

(b) RADIATION INTENSITY FOR INITIAL NOZZLE PRESSURE OF 50 MICRONS

Figure 10 INFLUENCE OF INITIAL NOZZLE PRESSURE ON STARTING PROCESS

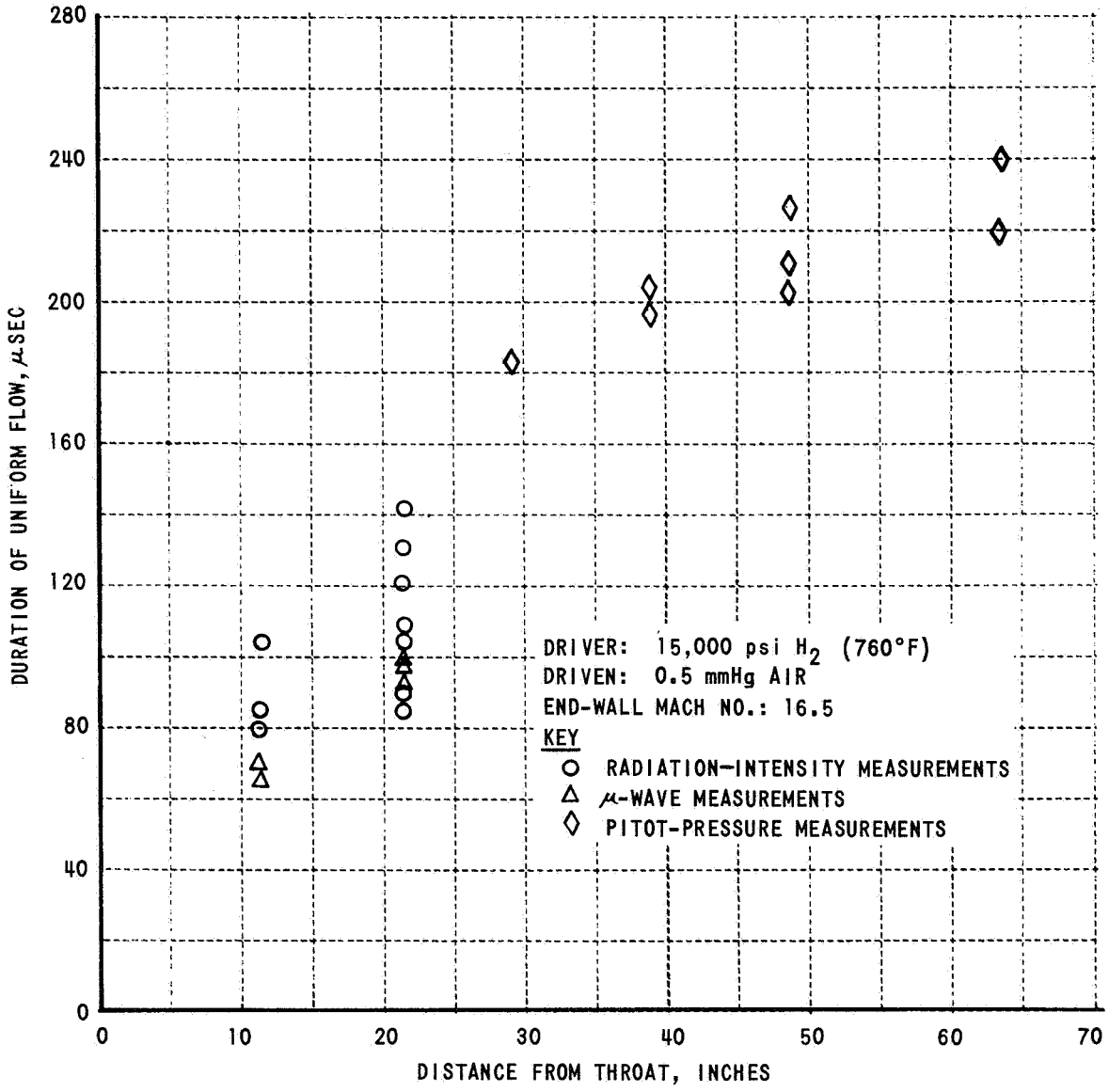

Figure 11 DURATION OF UNIFORM FLOW IN NOZZLE

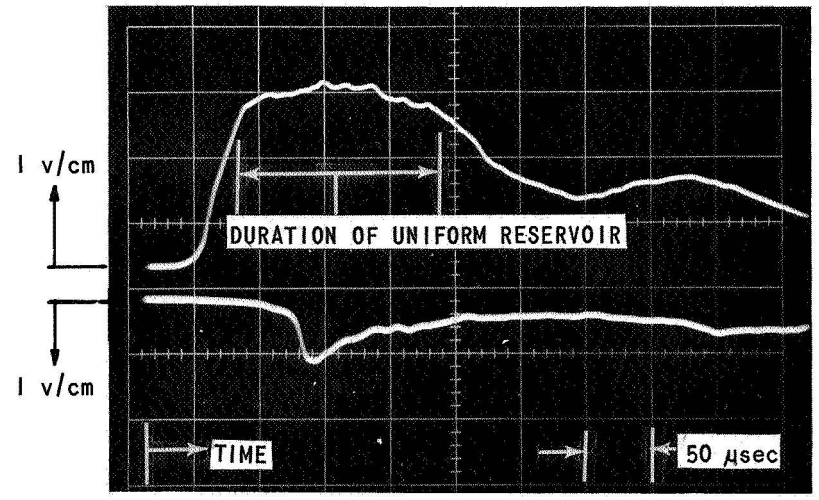

(a) RADIATION INTENSITY AT $\frac{3}{4}$-INCH FROM END WALL
RADIATION INTENSITY AT $3\frac{1}{4}$-INCHES FROM END WALL

DRIVER: 10,000 psi H_2 (760 °F)
DRIVEN: 10.0 mmHg AIR
END-WALL MACH NO.: 11.60

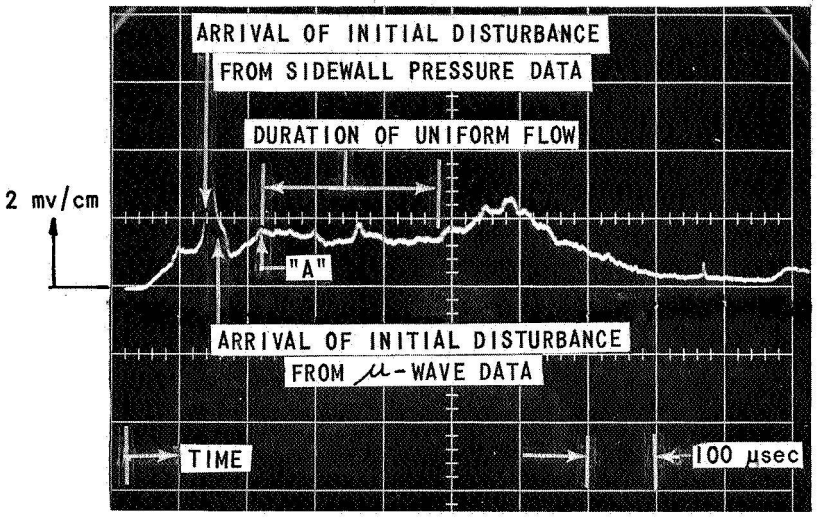

NOTE: "A" DENOTES INITIATION OF UNIFORM FLOW FROM INTEGRATION OF (u-a)

(b) RADIATION INTENSITY IN NOZZLE AT 21.5-INCHES FROM THROAT

Figure 12 RADIATION-INTENSITY MEASUREMENTS NORMAL TO AXIS IN SHOCK TUBE AND NOZZLE

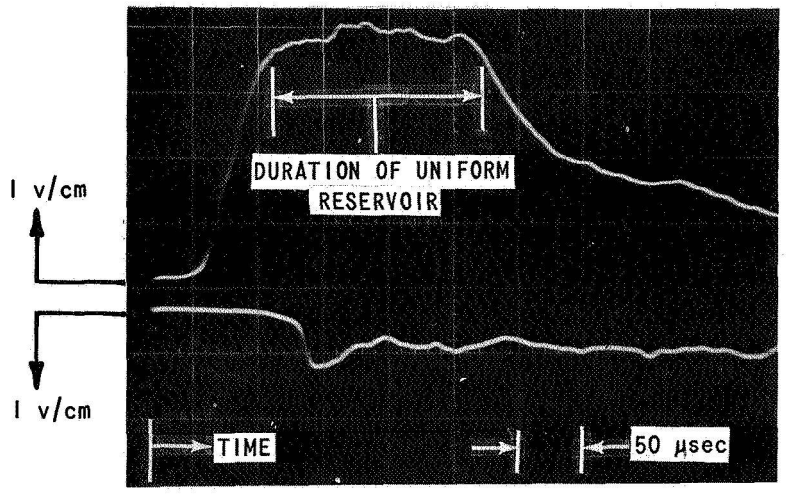

(a) RADIATION INTENSITY AT $\frac{3}{4}$-INCH FROM END WALL
RADIATION INTENSITY AT $3\frac{1}{4}$-INCHES FROM END WALL

DRIVER: 10,000 psi H_2 (760 °F)
DRIVEN: 10.0 mmHg AIR
END-WALL MACH NO.: 11.6

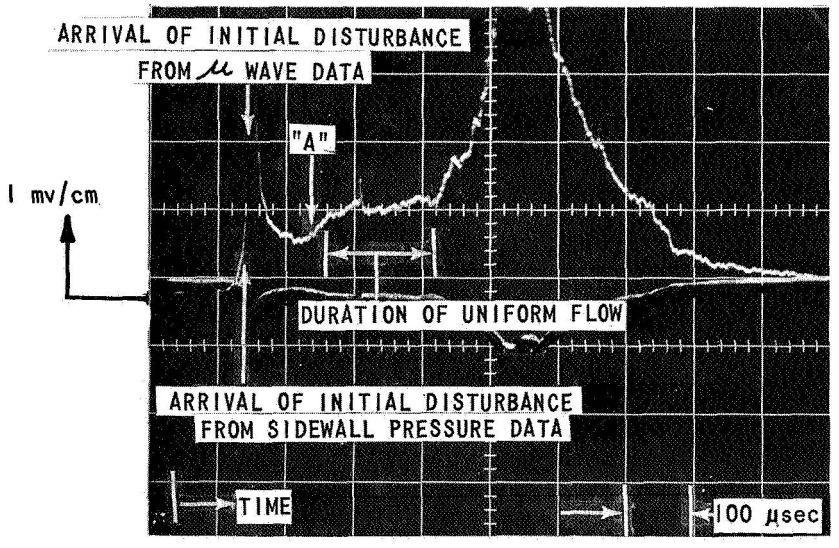

NOTE: "A" DENOTES INITIATION OF UNIFORM FLOW FROM INTEGRATION OF (u-a)

(b) RADIATION INTENSITY IN NOZZLE AT 21.5-INCHES FROM THROAT

Figure 13 RADIATION-INTENSITY MEASUREMENTS NORMAL TO AXIS IN SHOCK TUBE AND NOZZLE

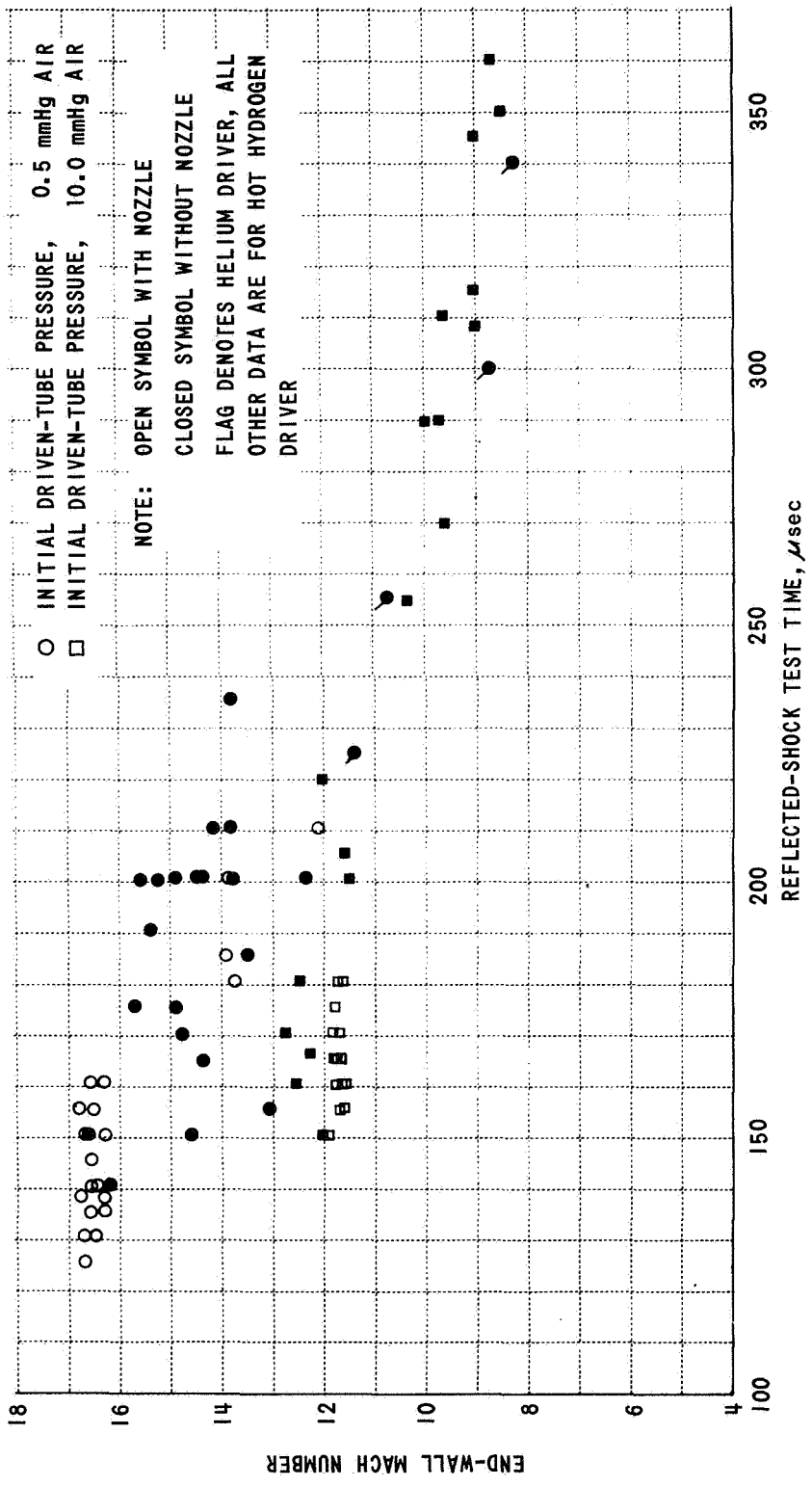

Figure 14 DURATION OF UNIFORM REFLECTED-SHOCK RESERVOIR WITH AND WITHOUT NOZZLE

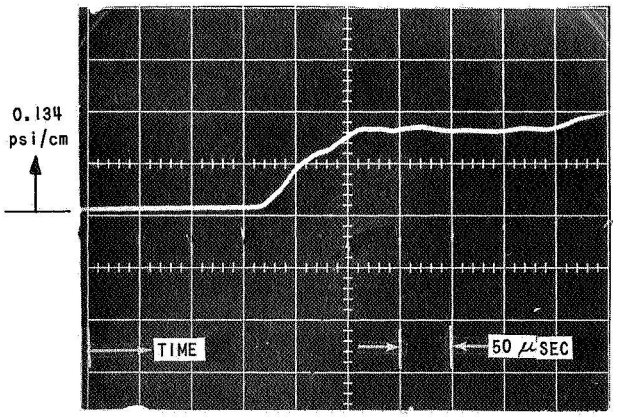

(a) PITOT PRESSURE ON CENTERLINE

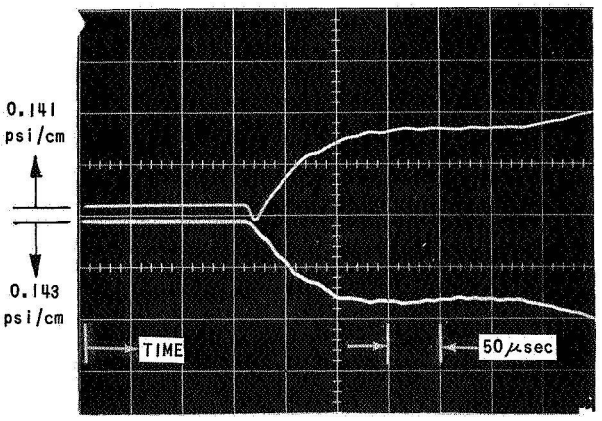

(b) PITOT PRESSURE AT -1.75-INCHES FROM CENTERLINE
PITOT PRESSURE AT +1.75-INCHES FROM CENTERLINE

DRIVER: 15,000 psi H_2 (760°F)
DRIVEN: 0.5 mmHg AIR
AXIAL DISTANCE FROM THROAT: 28 INCHES
END-WALL MACH NO.: 16.5

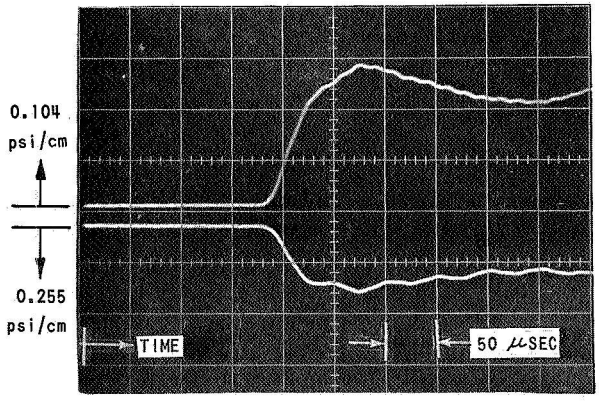

(c) PITOT PRESSURE AT -3-INCHES FROM CENTERLINE
PITOT PRESSURE AT +3-INCHES FROM CENTERLINE

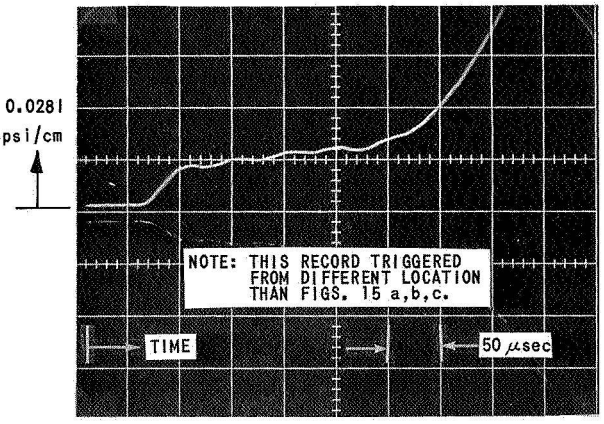

(d) PITOT PRESSURE AT +5-INCHES FROM CENTERLINE

Figure 15 RADIAL PITOT-PRESSURE MEASUREMENTS IN NOZZLE

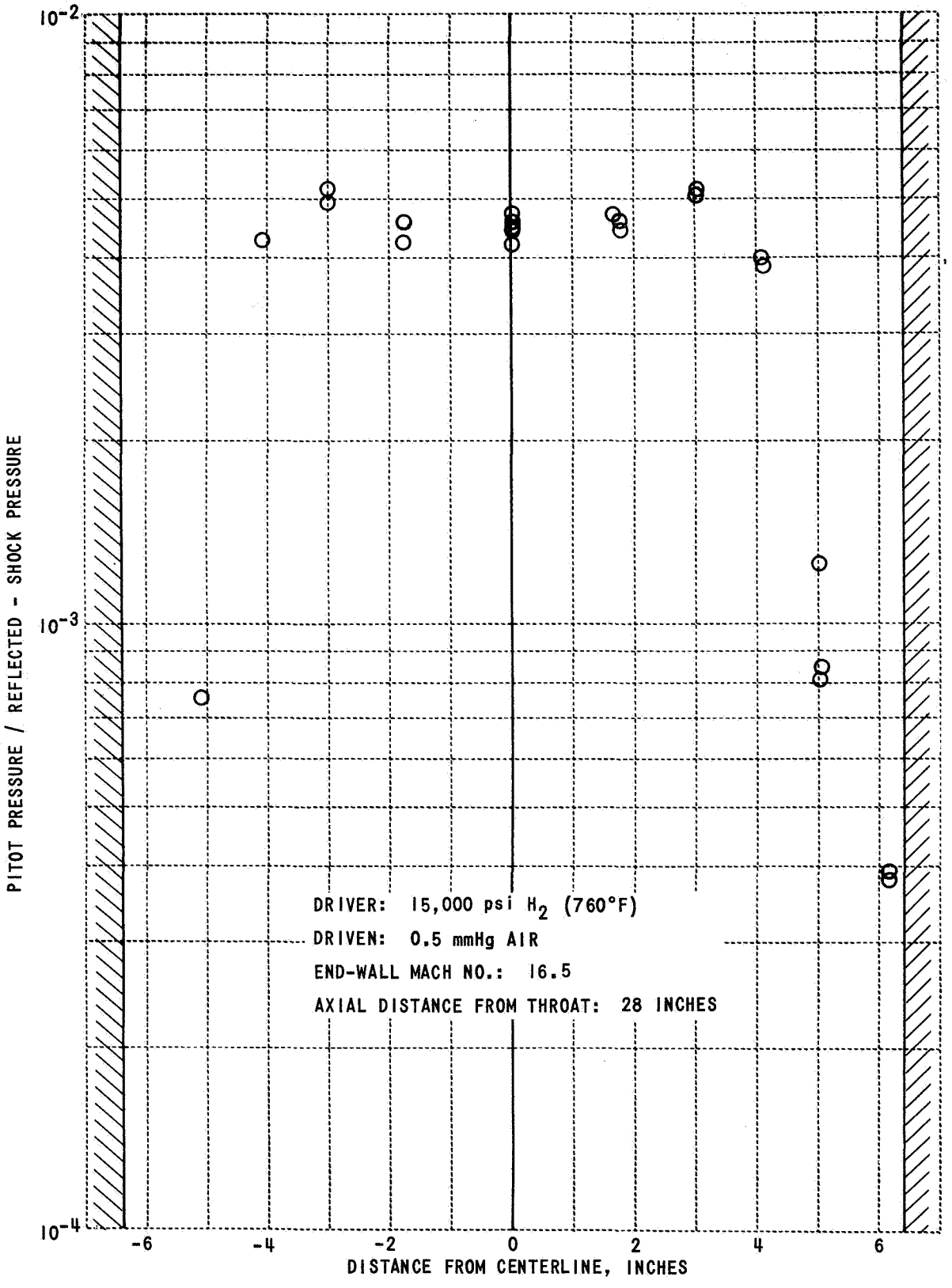

Figure 16 RADIAL PITOT-PRESSURE DISTRIBUTION

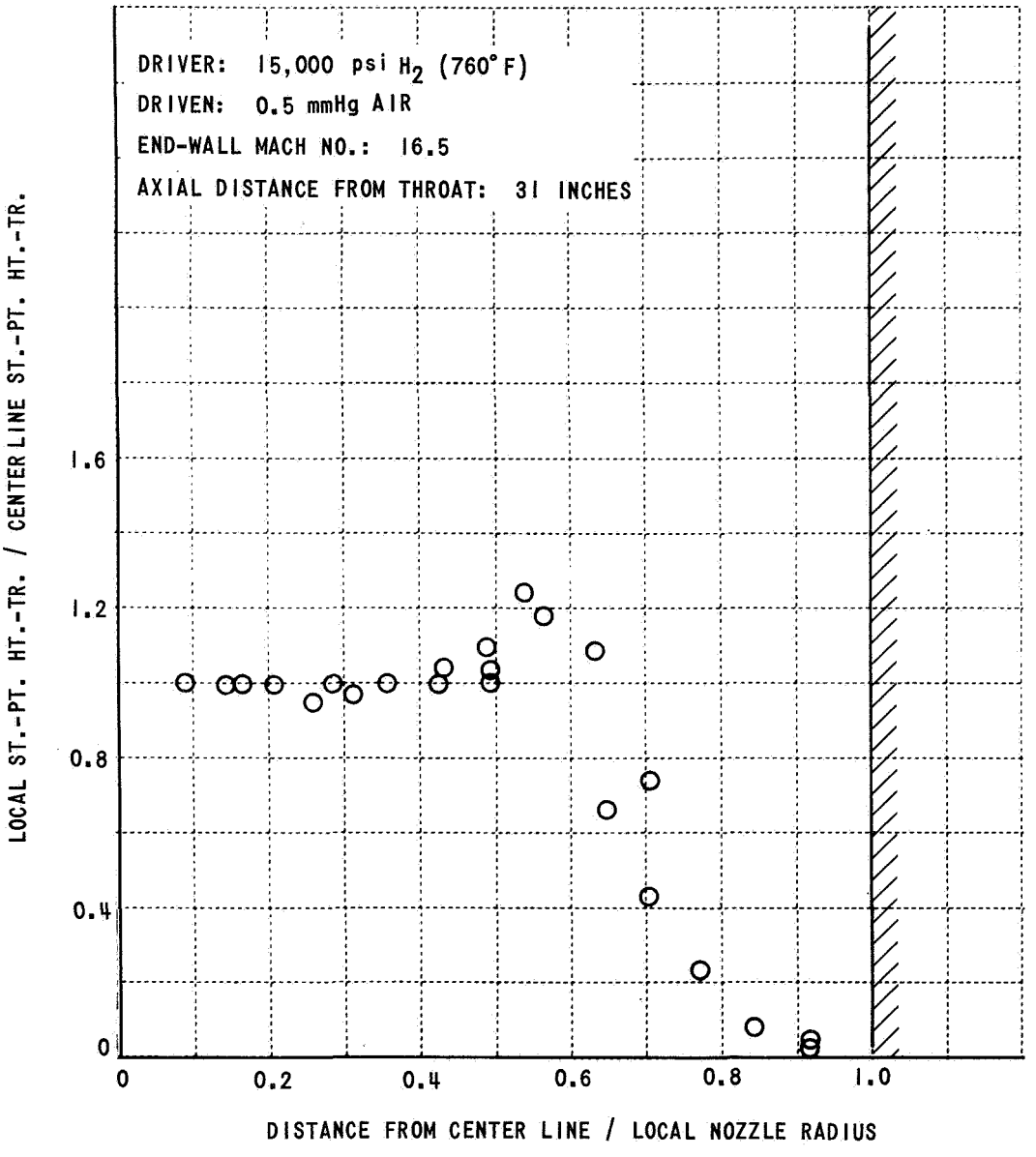

Figure 17 RADIAL STAGNATION-POINT HEAT-TRANSFER RATE DISTRIBUTION

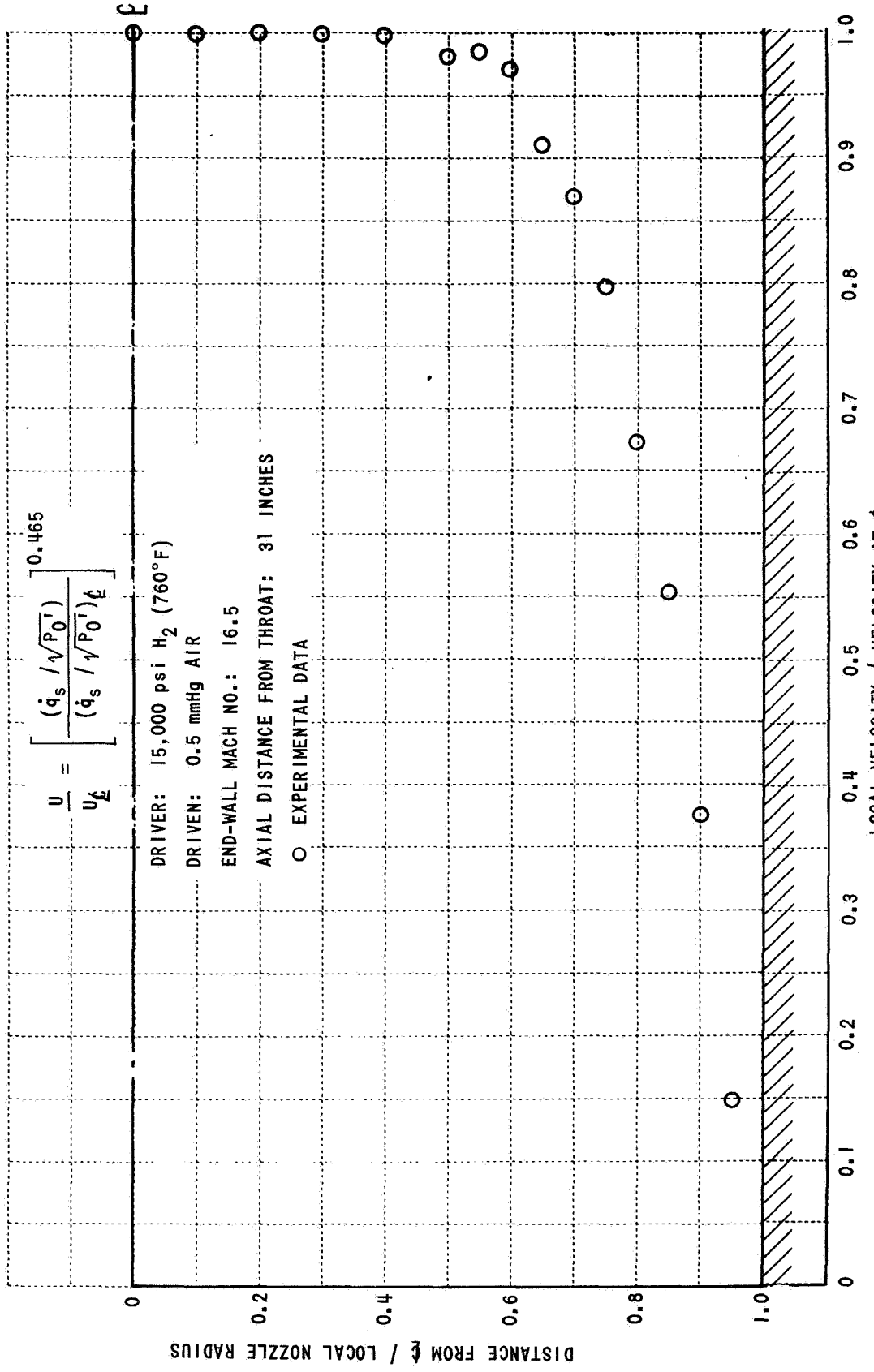

Figure 18 BOUNDARY-LAYER VELOCITY PROFILE IN NOZZLE DEDUCED FROM EXPERIMENTAL DATA

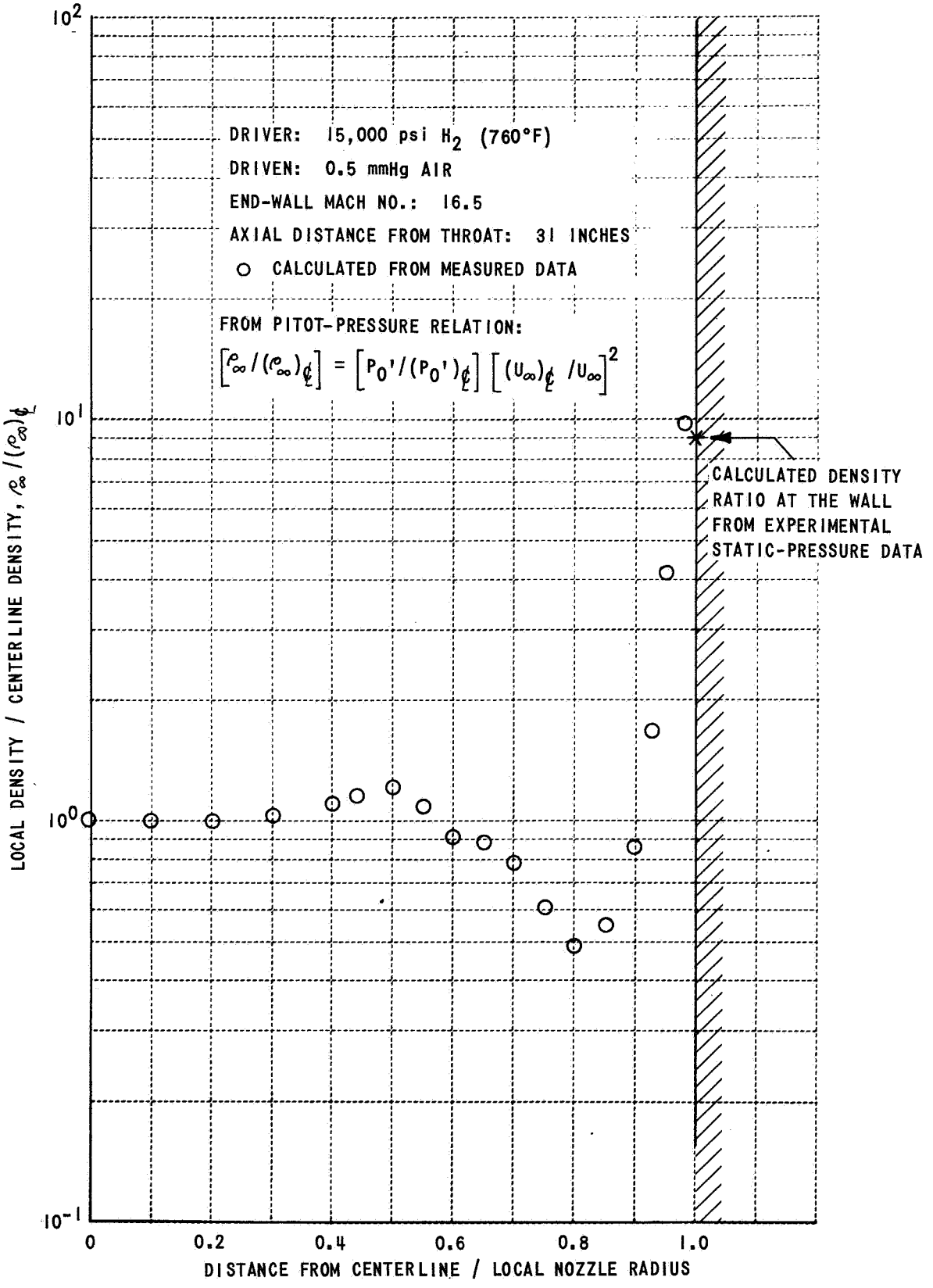

Figure 19 RADIAL DENSITY DISTRIBUTION

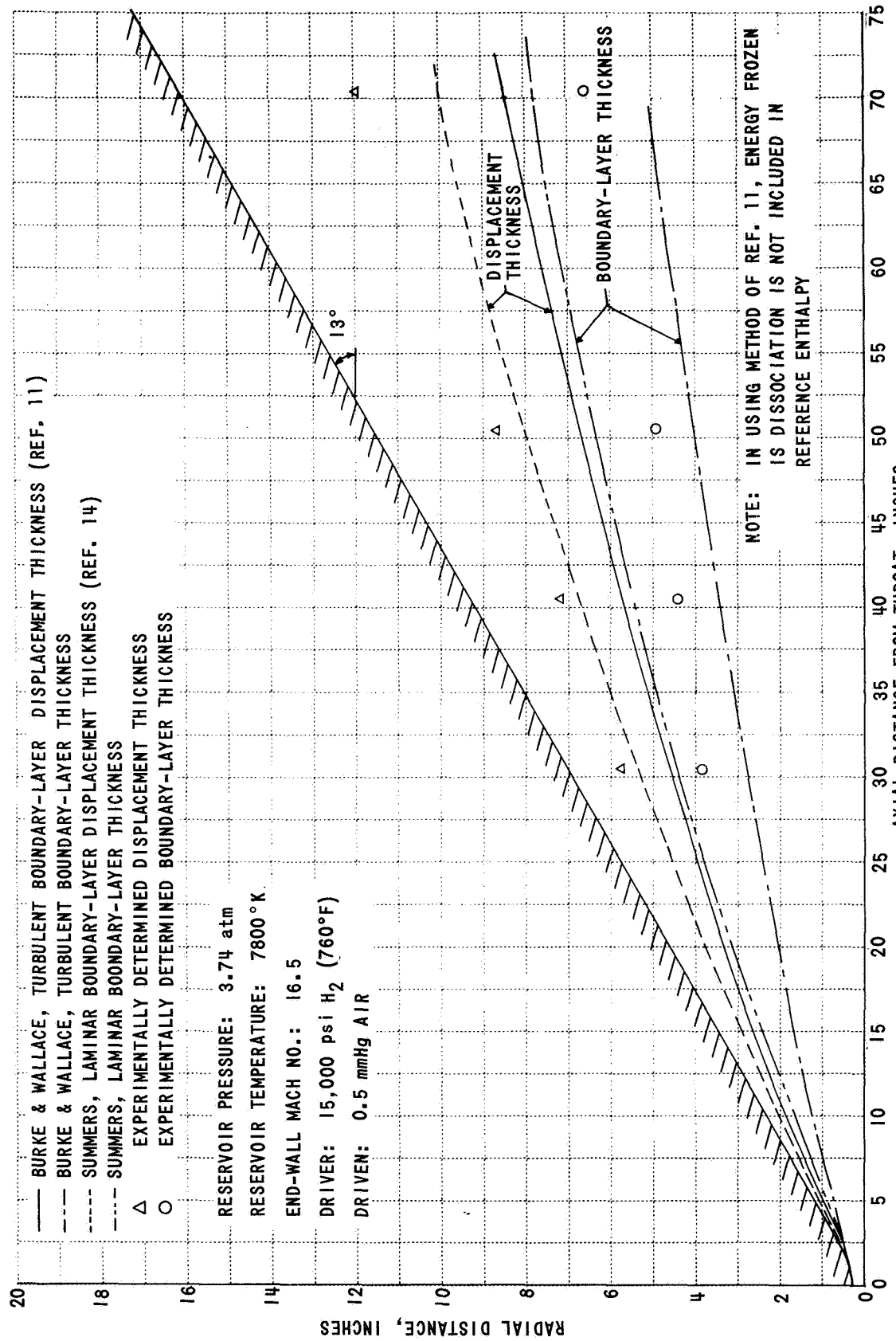

Figure 20 COMPARISON OF EXPERIMENTAL AND PREDICTED BOUNDARY LAYER AND DISPLACEMENT-THICKNESS GROWTH IN NOZZLE

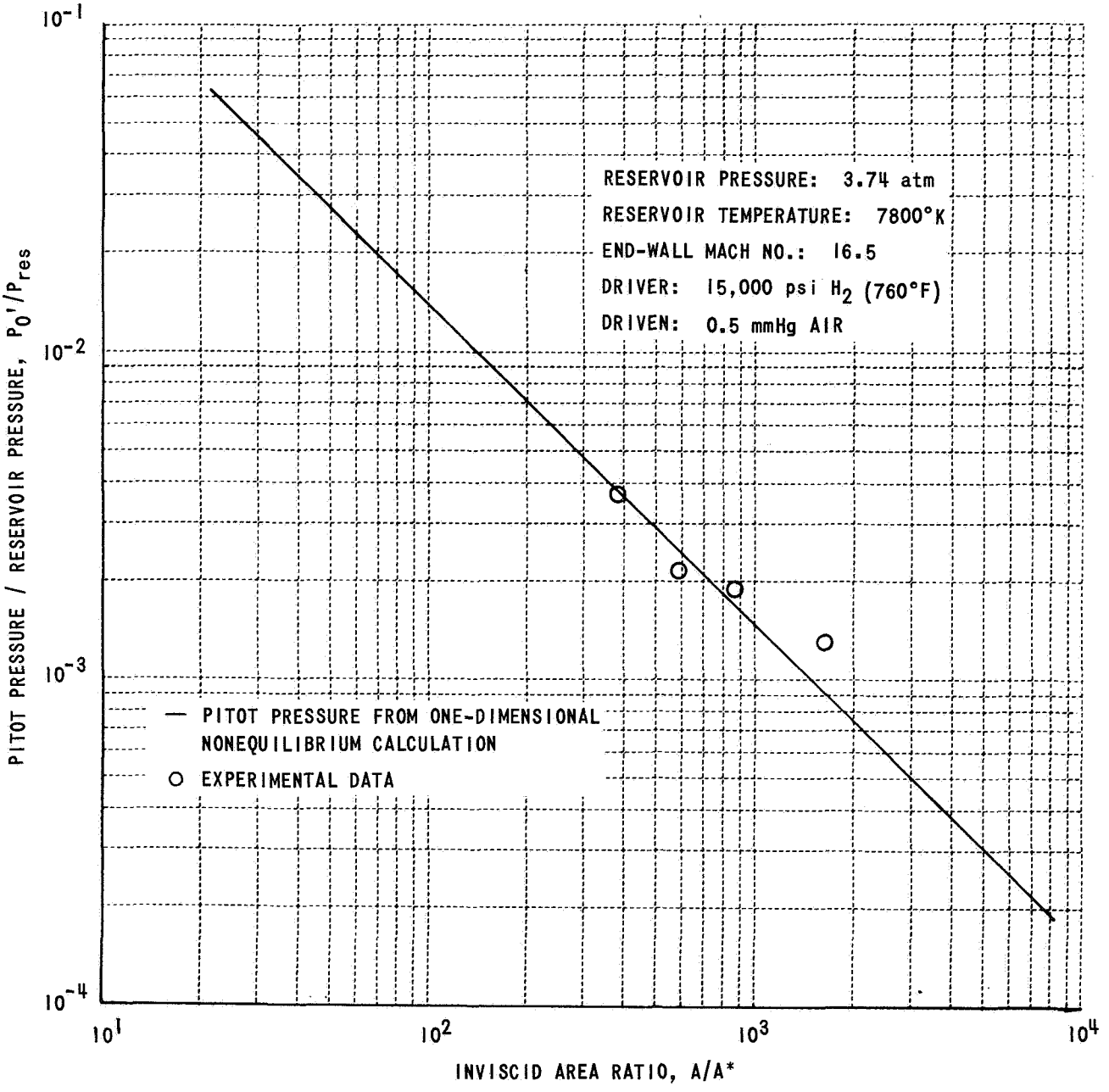

Figure 21 COMPARISON OF THEORETICAL AND EXPERIMENTAL PITOT PRESSURE IN NOZZLE

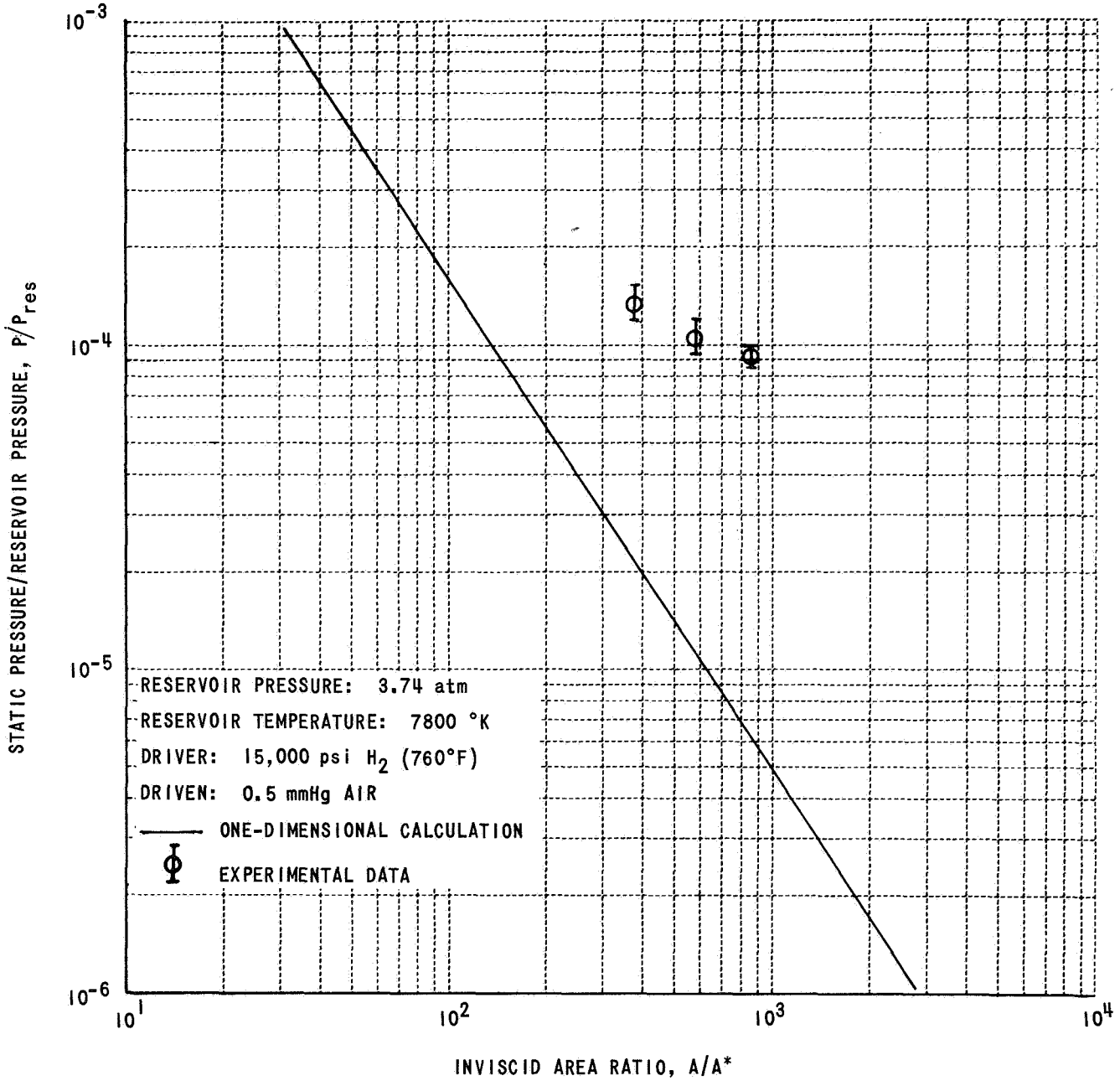

Figure 22 COMPARISON OF THEORETICAL AND EXPERIMENTAL STATIC-PRESSURE DISTRIBUTION IN NOZZLE

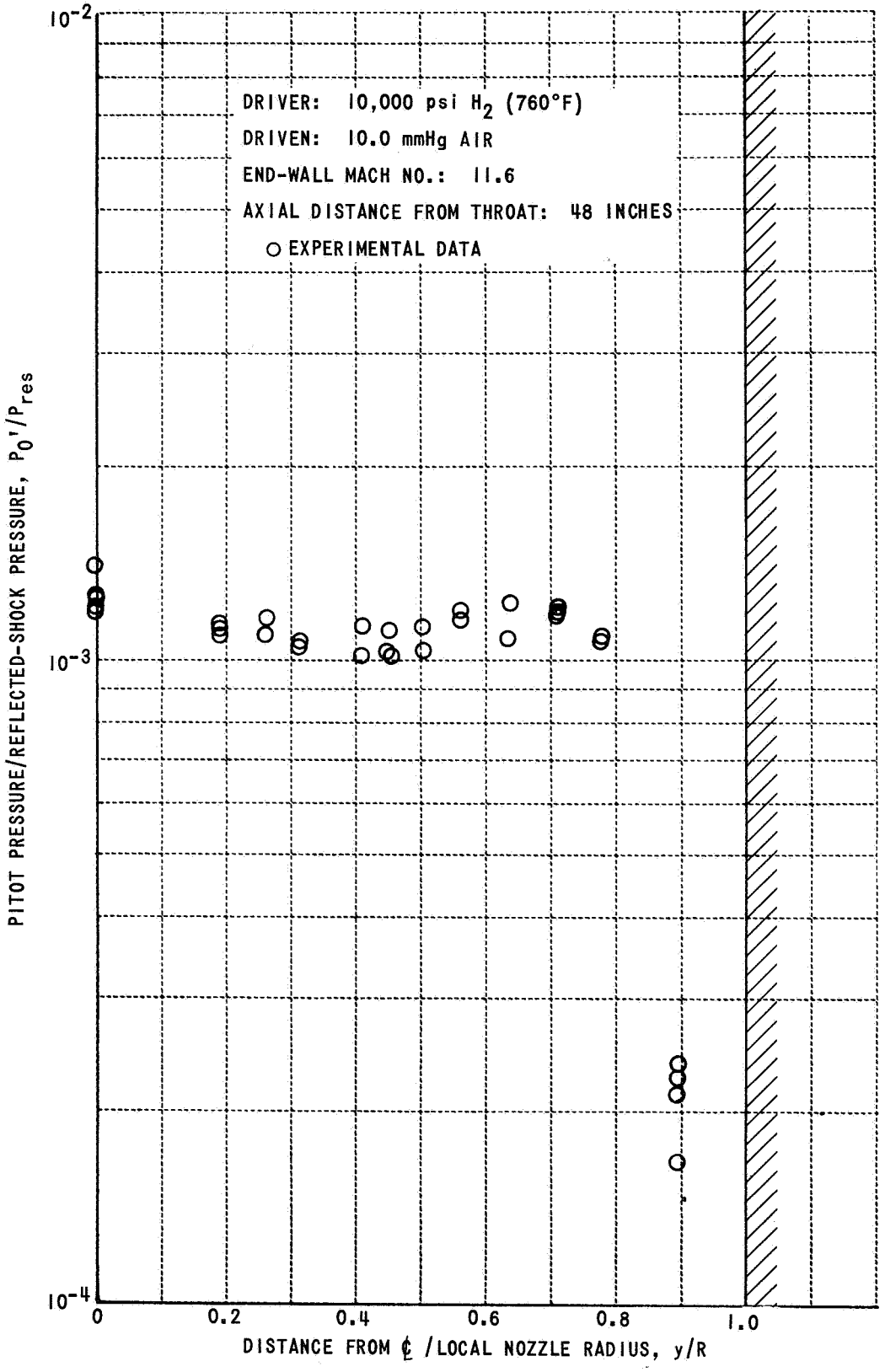

Figure 23 RADIAL PITOT-PRESSURE DISTRIBUTION IN NOZZLE

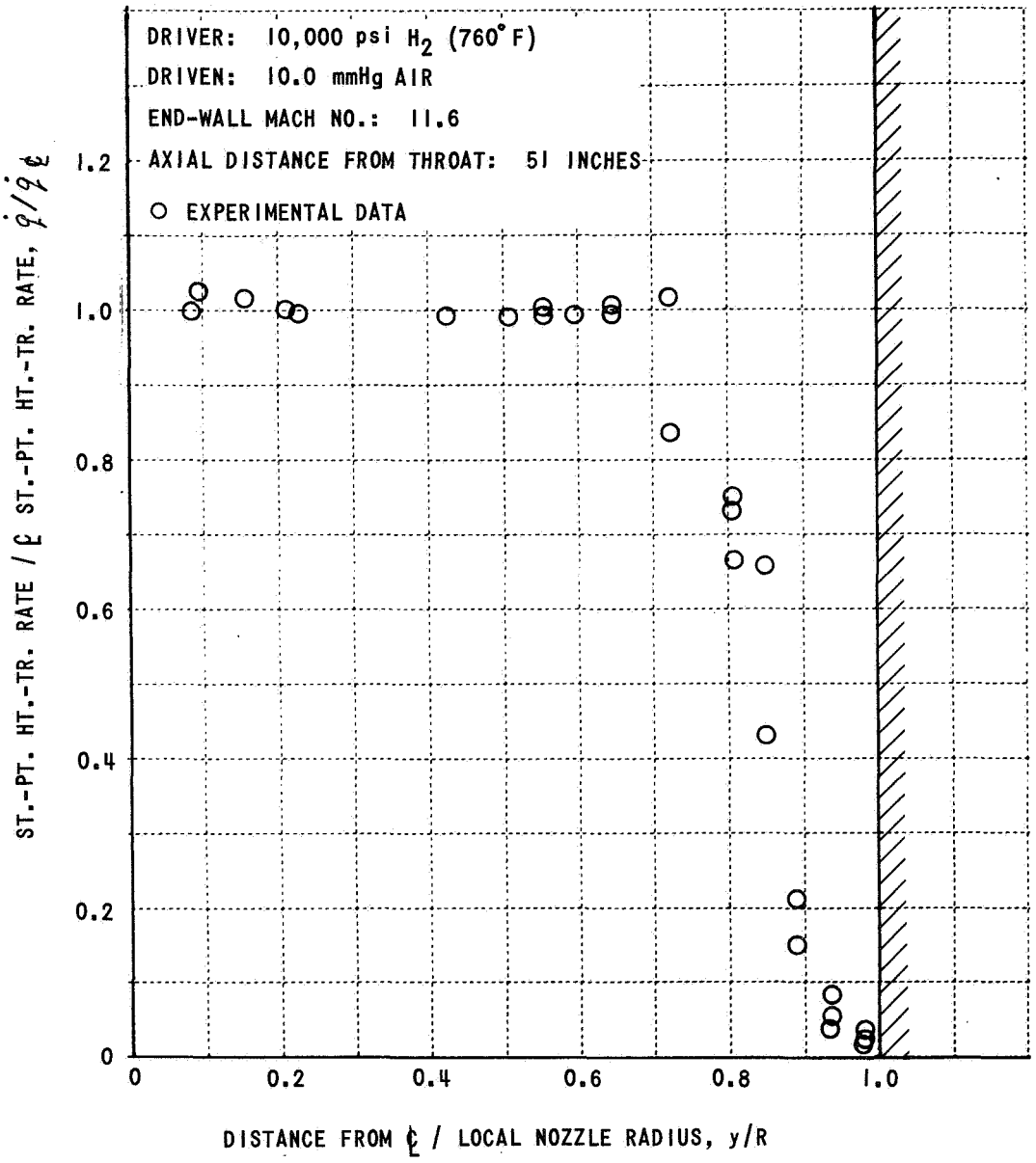

Figure 24 RADIAL STAGNATION-POINT HEAT-TRANSFER RATE DISTRIBUTION IN NOZZLE

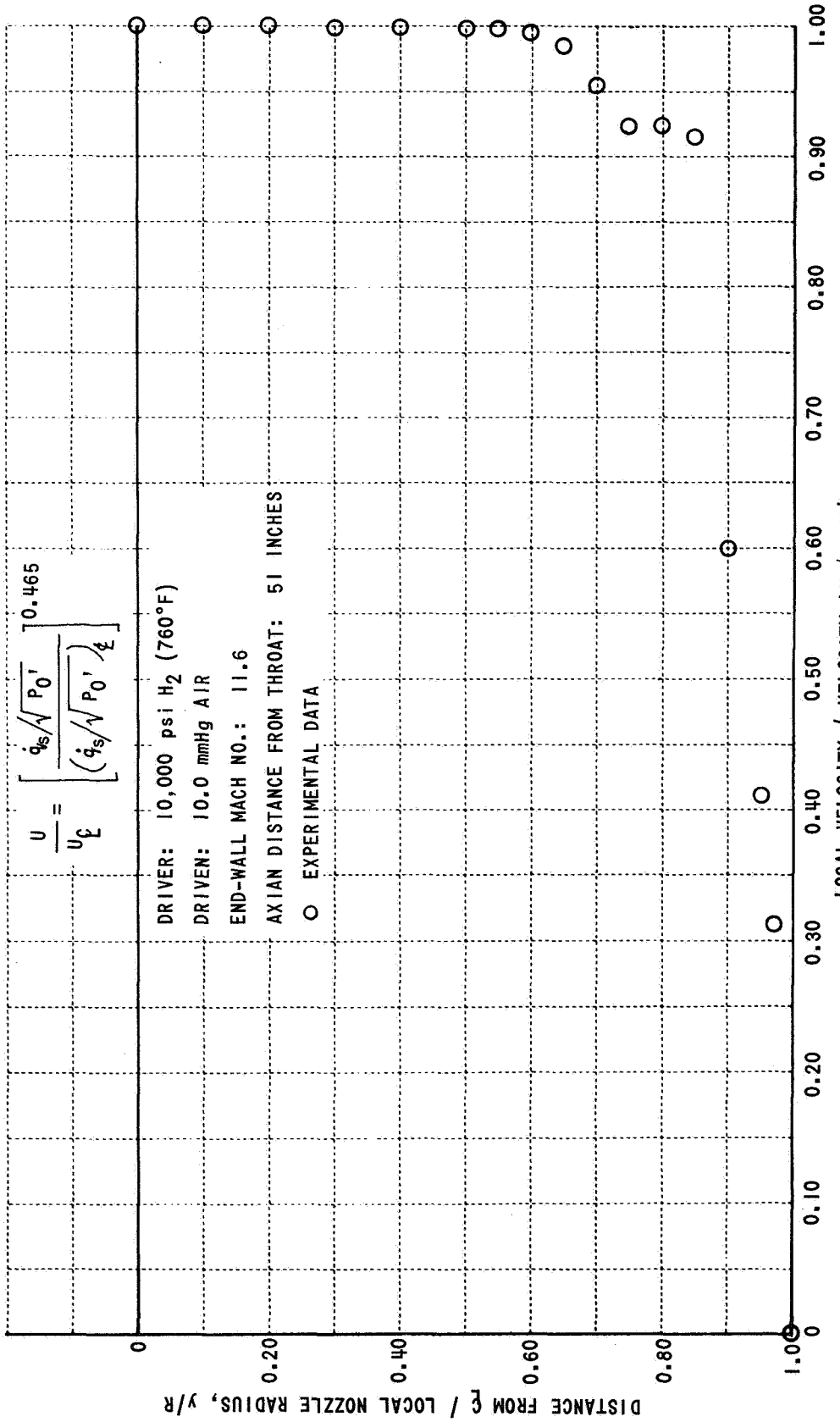

Figure 25 BOUNDARY-LAYER VELOCITY PROFILE IN NOZZLE DEDUCED FROM EXPERIMENTAL DATA

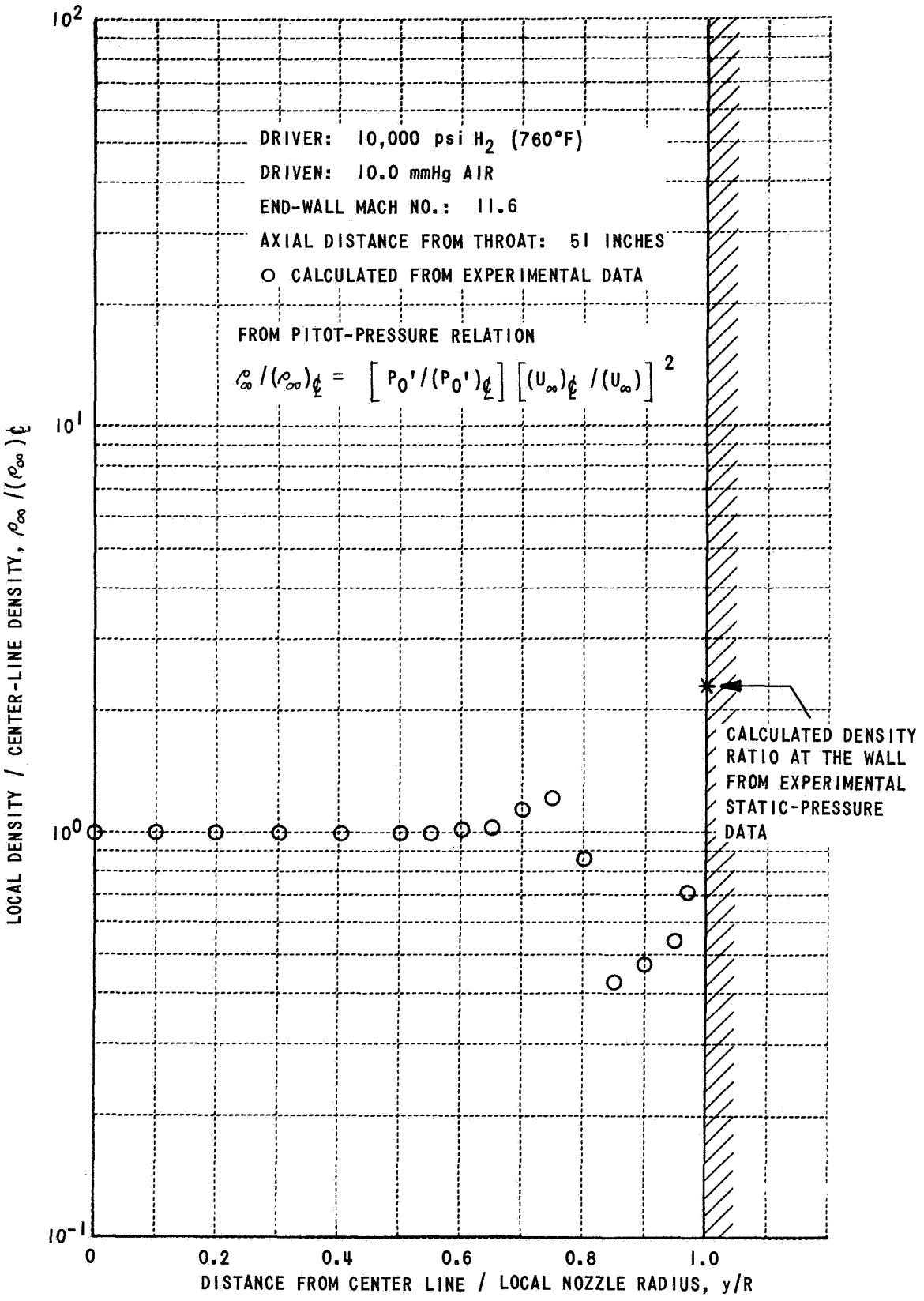

Figure 26 RADIAL DENSITY DISTRIBUTION

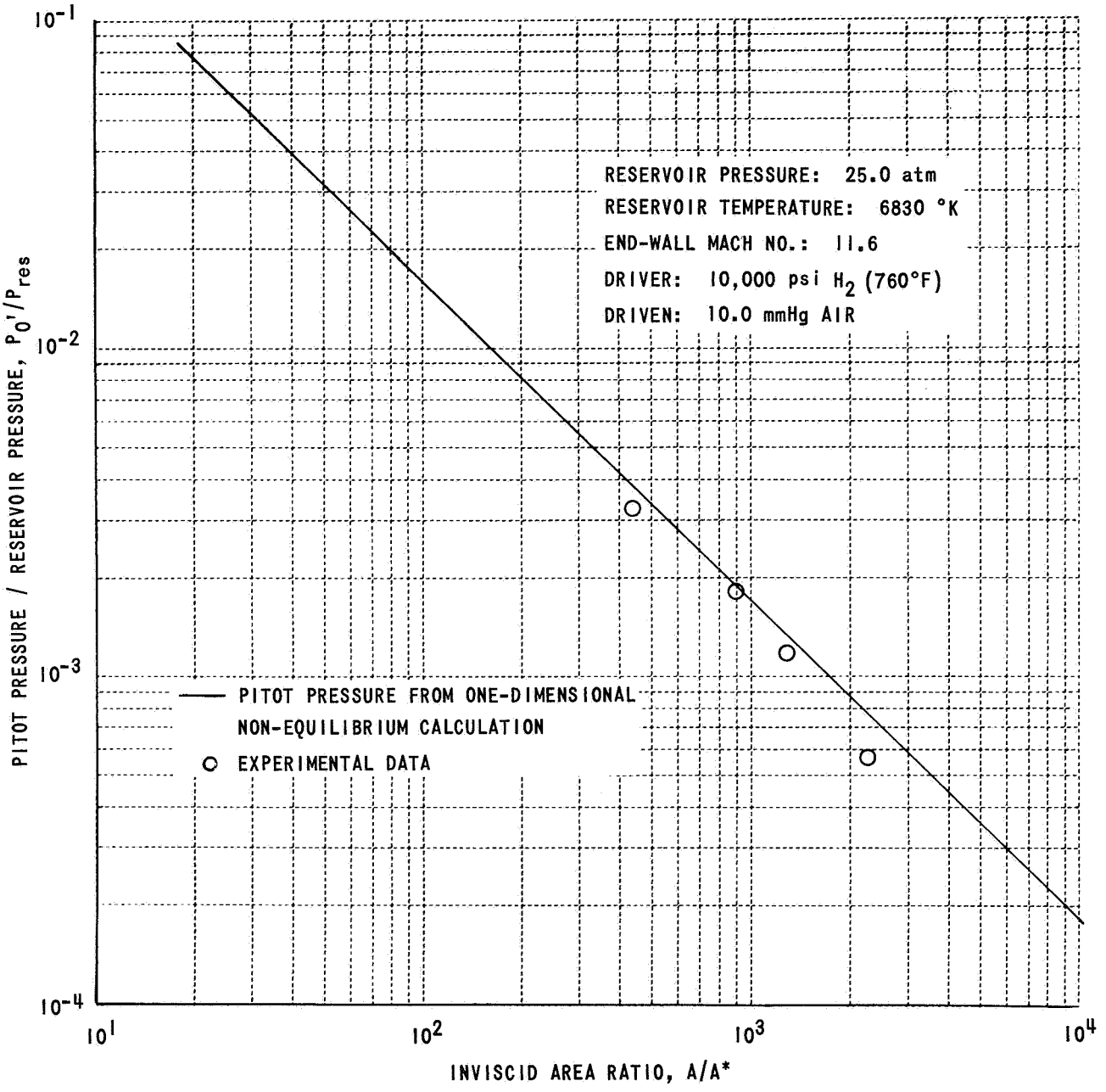

Figure 27 COMPARISON OF THEORETICAL AND EXPERIMENTAL PITOT PRESSURE IN NOZZLE

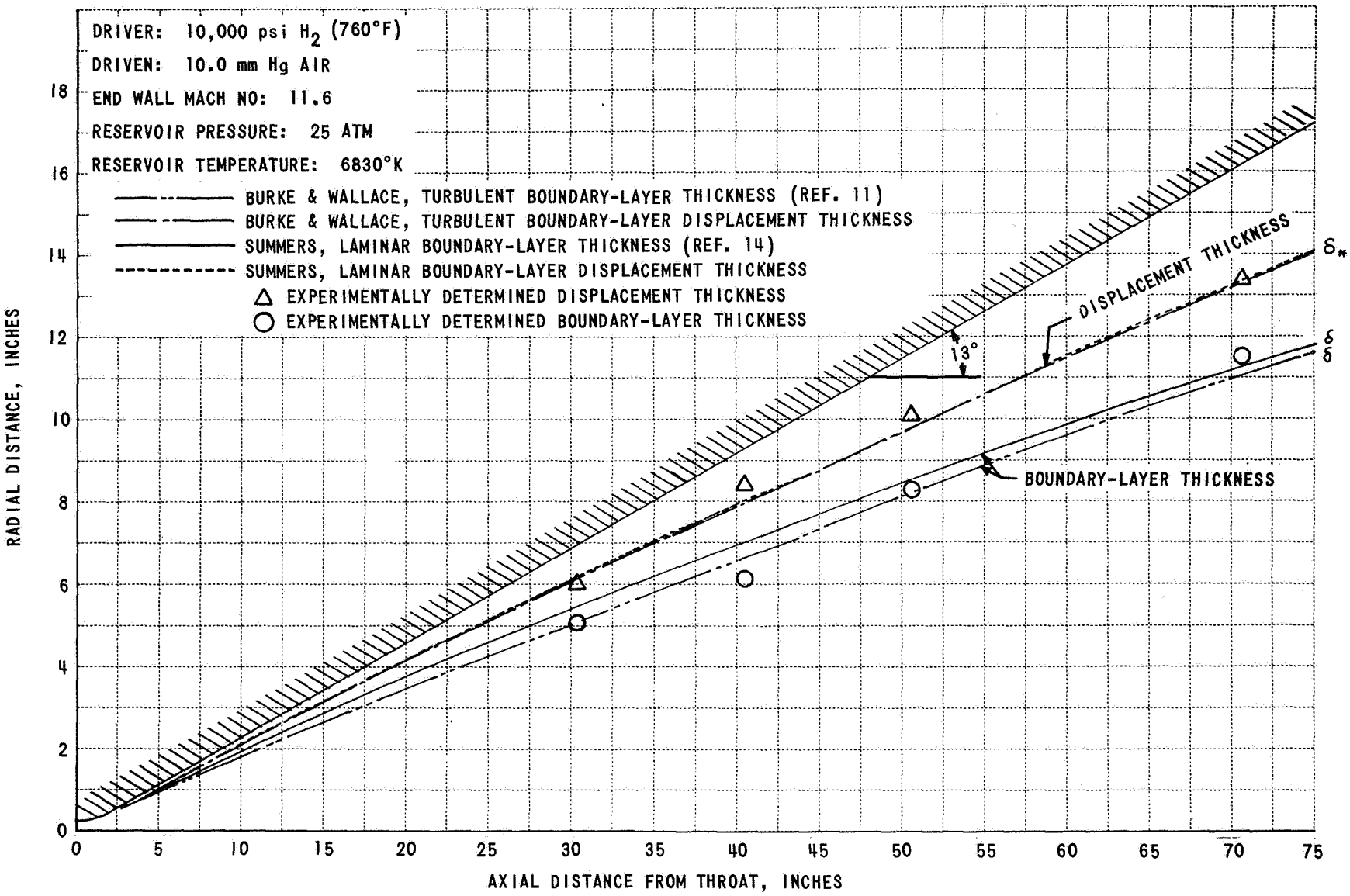

Figure 28 COMPARISON OF EXPERIMENTAL AND PREDICTED BOUNDARY LAYER AND DISPLACEMENT-THICKNESS GROWTH IN NOZZLE

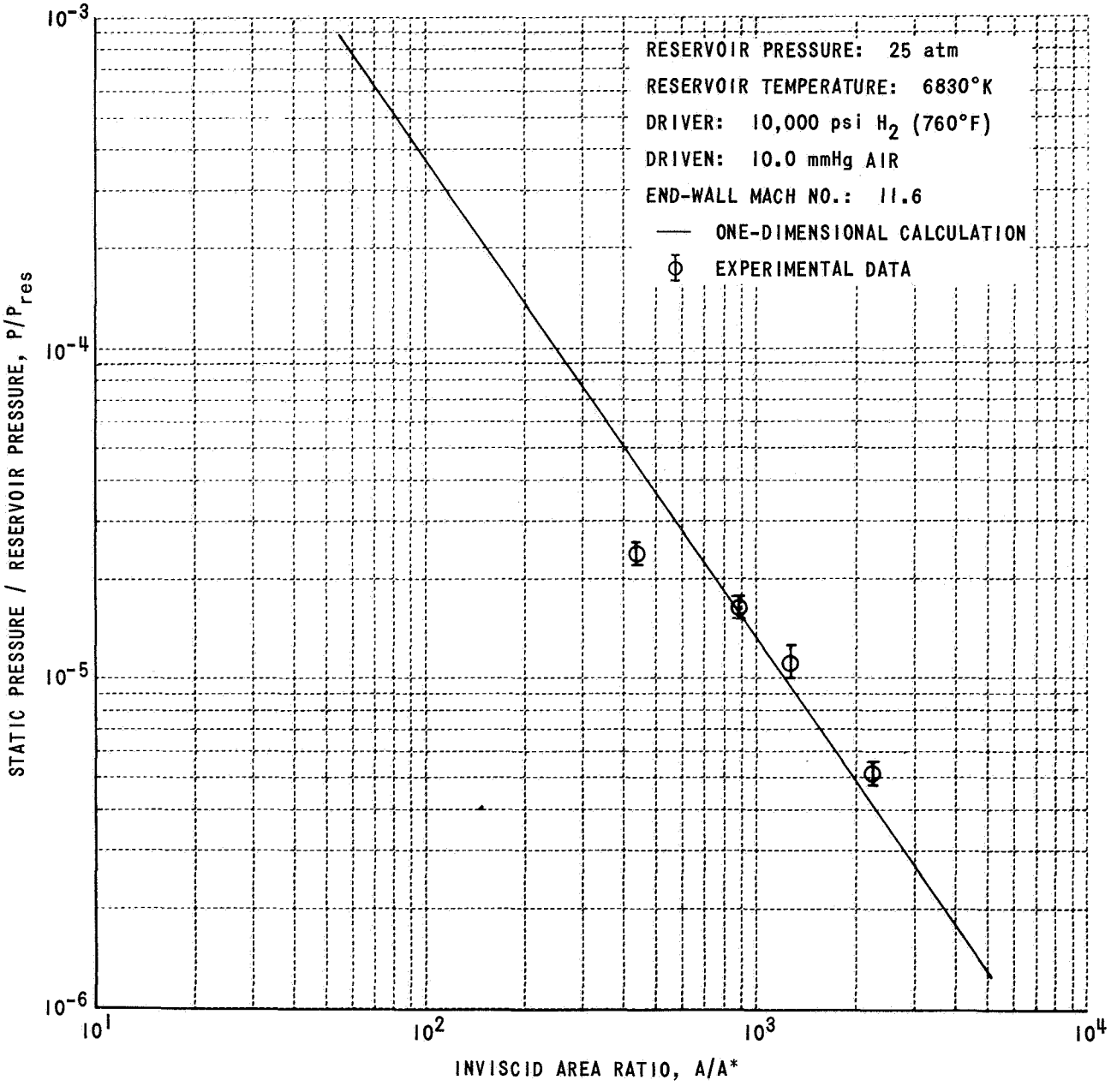

Figure 29 COMPARISON OF THEORETICAL AND EXPERIMENTAL STATIC-PRESSURE DISTRIBUTION IN NOZZLE

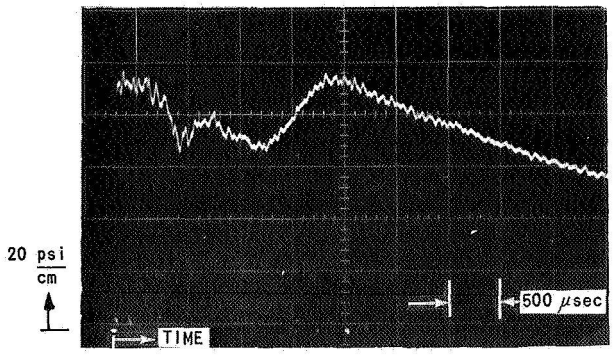

(a) END-WALL PRESSURE

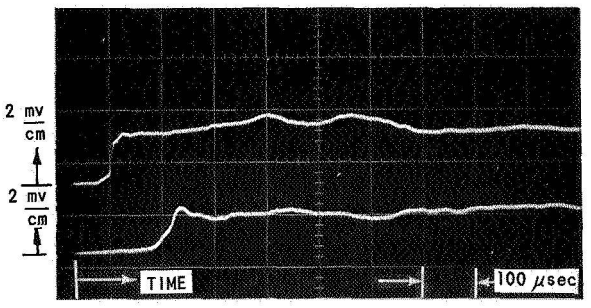

(b) RADIATION INTENSITY $\frac{3}{4}$-INCH FROM END WALL
RADIATION INTENSITY $3\frac{1}{4}$-INCHES FROM END WALL

DRIVER: 800 psi H_2 (760°F)
DRIVEN: 10.0 mmHg AIR
END-WALL MACH NO.: 7.3

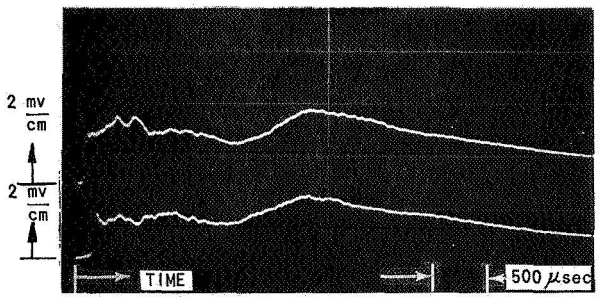

(c) RADIATION INTENSITY $\frac{3}{4}$-INCH FROM END WALL
RADIATION INTENSITY $3\frac{1}{4}$-INCHES FROM END WALL

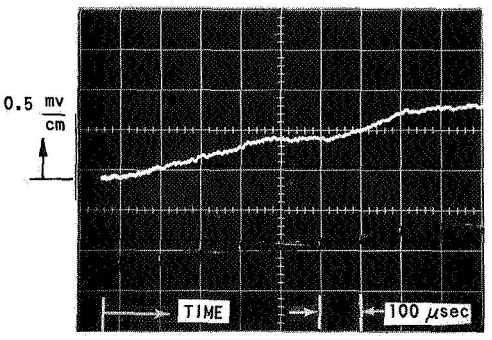

(d) END-WALL RADIATION INTENSITY

Figure 30 REFLECTED-SHOCK MEASUREMENTS AT RELATIVELY LOW MACH NUMBER

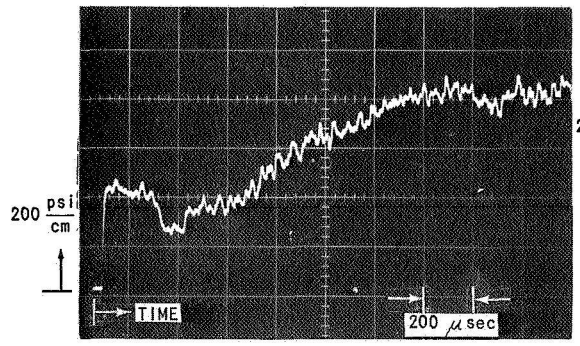

(a) END-WALL PRESSURE

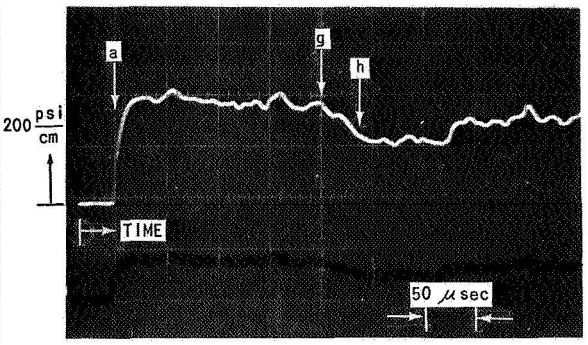

(b) END WALL PRESSURE

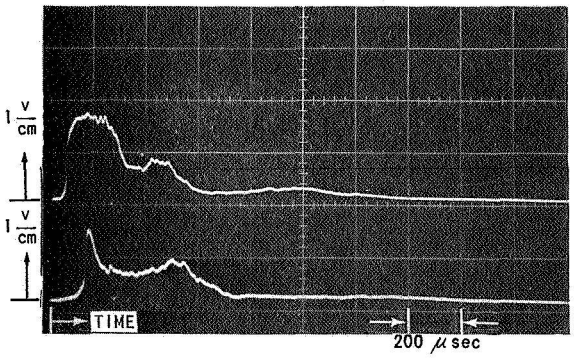

(c) RADIATION INTENSITY $\frac{3}{4}$ INCH FROM END WALL
RADIATION INTENSITY $3\frac{1}{4}$ INCHES FROM END WALL

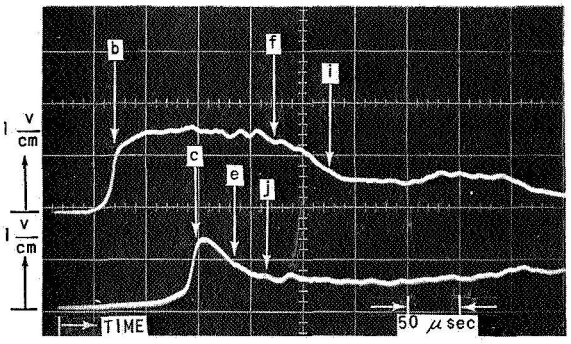

(d) RADIATION INTENSITY $\frac{3}{4}$ INCH FROM END WALL
RADIATION INTENSITY $3\frac{1}{4}$ INCHES FROM END WALL

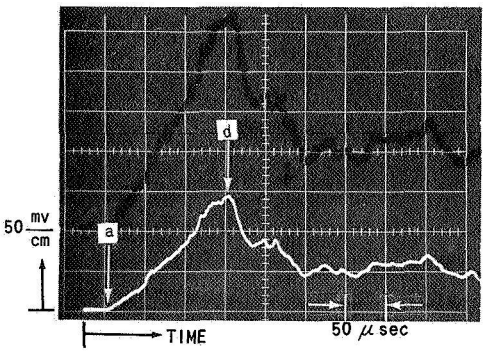

(e) END WALL RADIATION INTENSITY

DRIVER: 15,000 psi H_2 (760° F)
DRIVEN: 10.0 mm Hg AIR
END-WALL MACH NO.: 12.2

Figure 31 SHOCK-TUBE MEASUREMENTS AT RELATIVELY HIGH MACH NUMBER

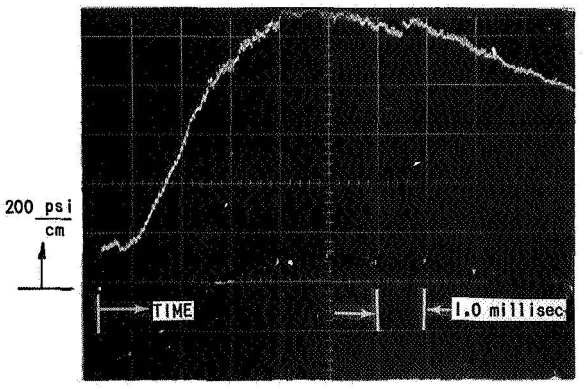

(a) END-WALL PRESSURE

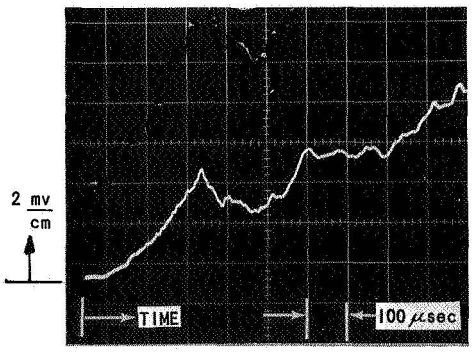

(b) END-WALL RADIATION INTENSITY

DRIVER: 15,000 psi He (760°F)
DRIVEN: 10.0 mmHg AIR
END-WALL MACH NO. : 8.6

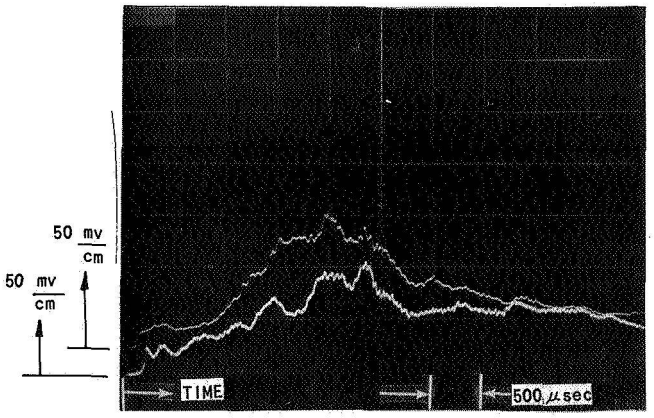

(c) RADIATION INTENSITY $\frac{3}{4}$-INCH FROM END WALL
RADIATION INTENSITY $3\frac{1}{4}$-INCHES FROM END WALL

Figure 32 INFLUENCE OF HELIUM DRIVER GAS ON REFLECTED-SHOCK GAS DYNAMICS

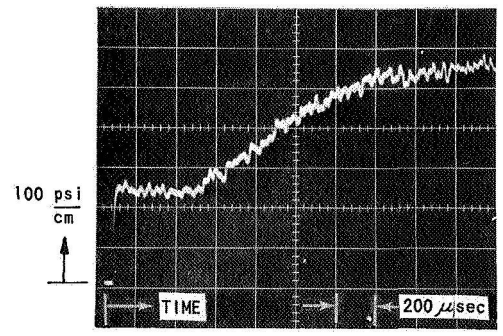

(a) END-WALL PRESSURE

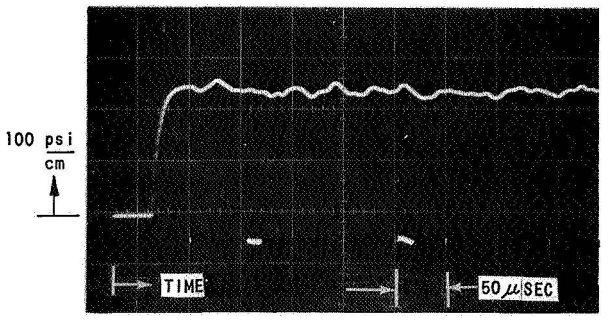

(b) END-WALL PRESSURE

DRIVER: 6700 psi H_2 (760°F)
DRIVEN: 10.0 mmHg NITROGEN
END-WALL MACH NO. : 10.6

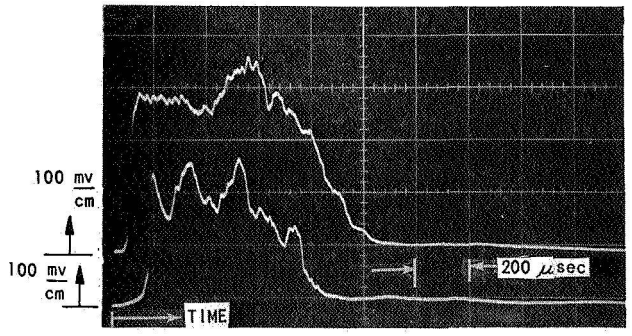

(c) RADIATION INTENSITY $\frac{3}{4}$-INCH FROM END WALL
RADIATION INTENSITY $3\frac{1}{4}$-INCHES FROM END WALL

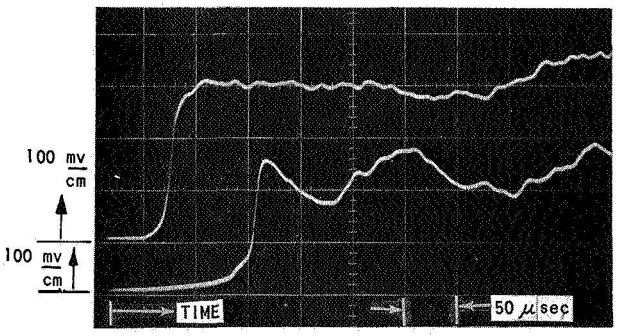

(d) RADIATION INTENSITY $\frac{3}{4}$-INCH FROM END WALL
RADIATION INTENSITY $3\frac{1}{4}$-INCHES FROM END WALL

Figure 33 INFLUENCE OF DRIVEN-TUBE GAS ON REFLECTED-SHOCK MEASUREMENTS

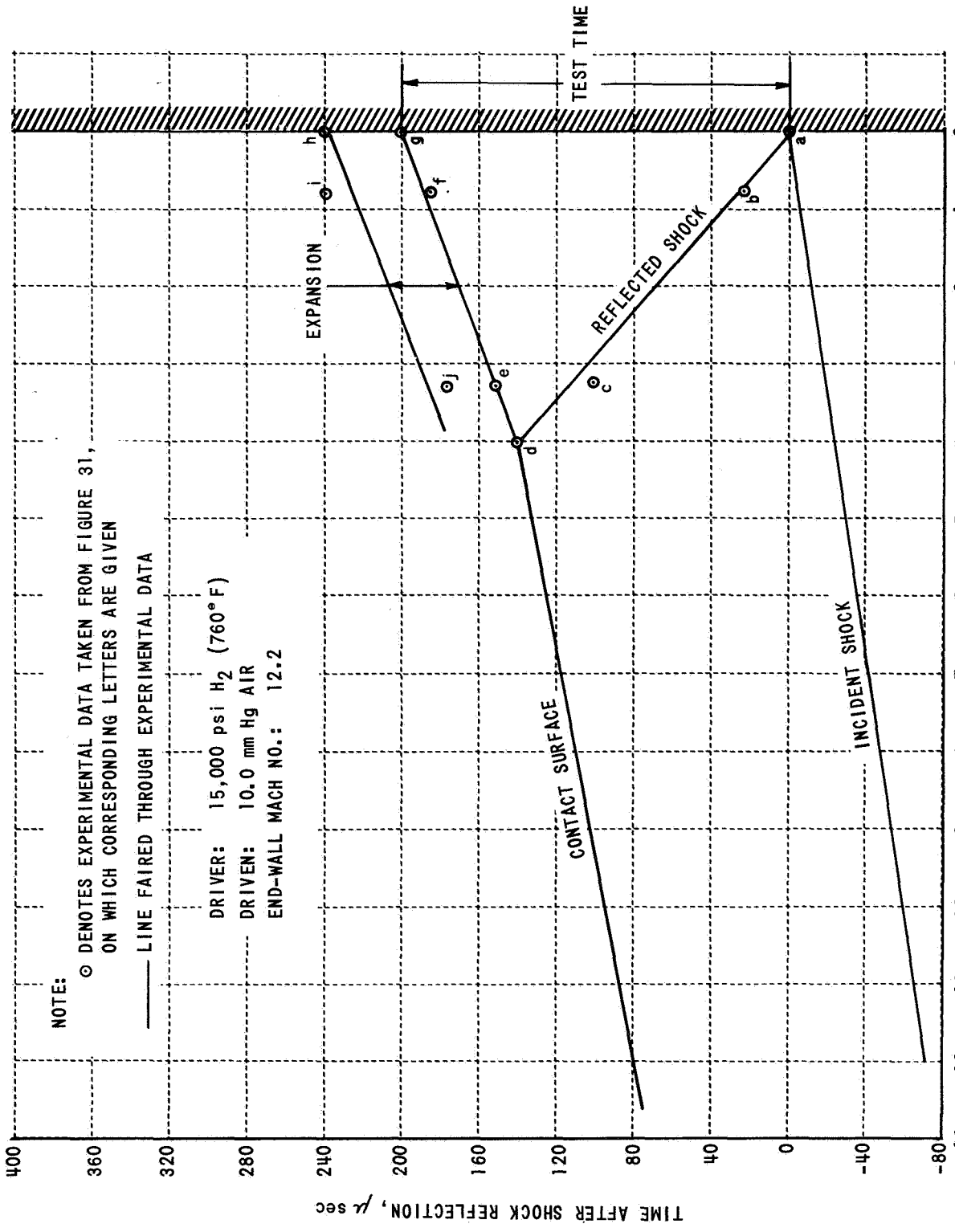

Figure 34 WAVE DIAGRAM CONSTRUCTED FROM EXPERIMENTAL DATA

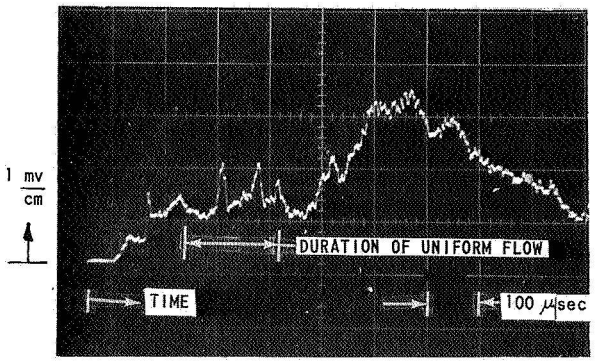

(a) RADIATION INTENSITY AT 11.5-INCHES FROM THROAT

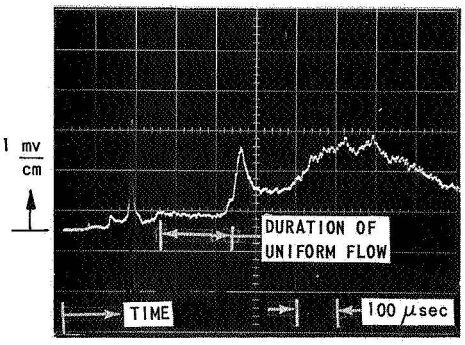

(b) RADIATION INTENSITY AT 21.5-INCHES FROM THROAT

DRIVER: 4000 psi H_2 (760°F)
DRIVEN: 10.0 mmHg AIR
END-WALL MACH NO.: 9.9

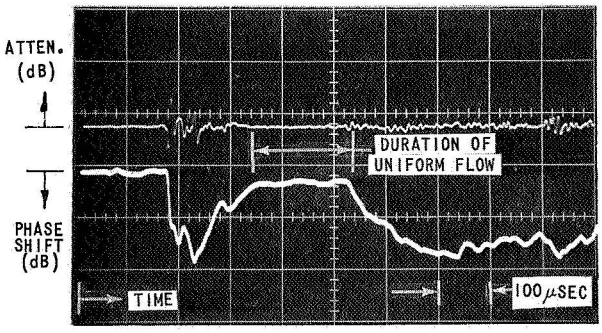

(c) 35GHz MICROWAVE INTERFEROMETER DATA AT 21.5-INCHES FROM THROAT

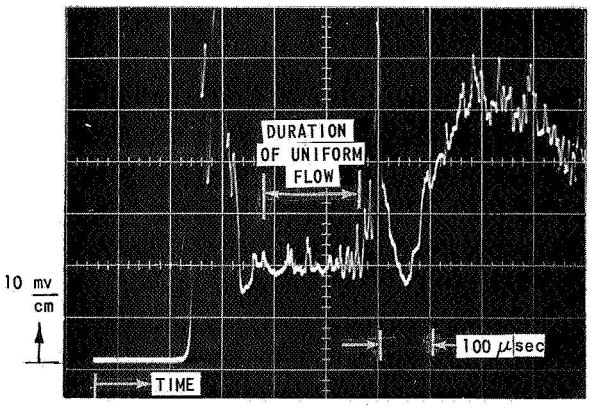

(d) LANGMUIR PROBE OUTPUT ACROSS 100 Ω RESISTOR AT 26.4-INCHES FROM THROAT (+3 VOLT BIAS)

Figure 35 RADIATION INTENSITY AND ELECTRON DENSITY MEASUREMENTS IN NOZZLE

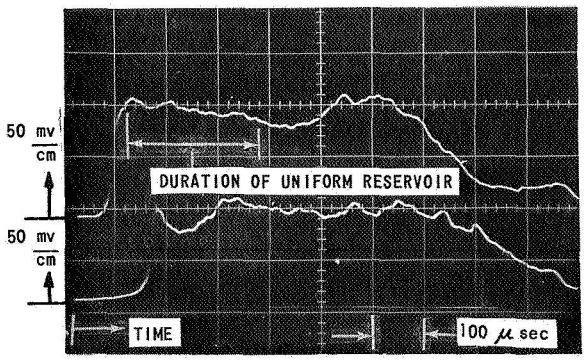

(a) RADIATION INTENSITY $\frac{3}{4}$-INCH FROM END WALL
RADIATION INTENSITY $3\frac{1}{4}$-INCHES FROM END WALL

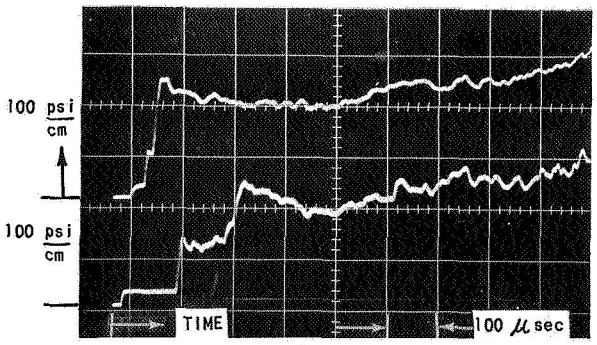

(b) PRESSURE $\frac{3}{4}$-INCH FROM END WALL
PRESSURE $3\frac{1}{4}$-INCHES FROM END WALL

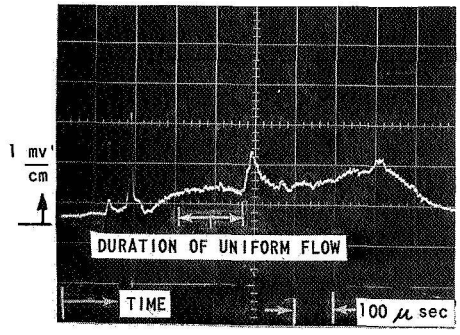

(c) RADIATION INTENSITY AT 21.5-INCHES FROM THROAT

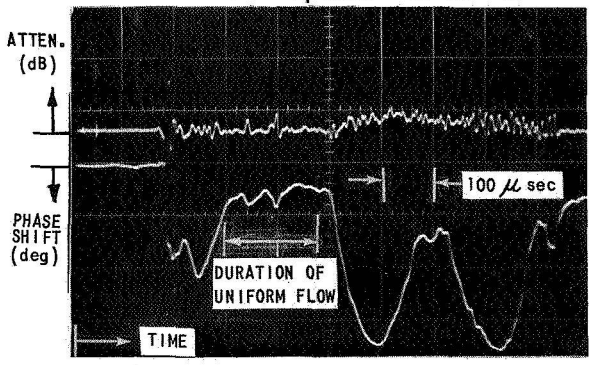

(d) 35 GHz MICROWAVE INTERFEROMETER DATA AT 21.5-INCHES FROM THROAT

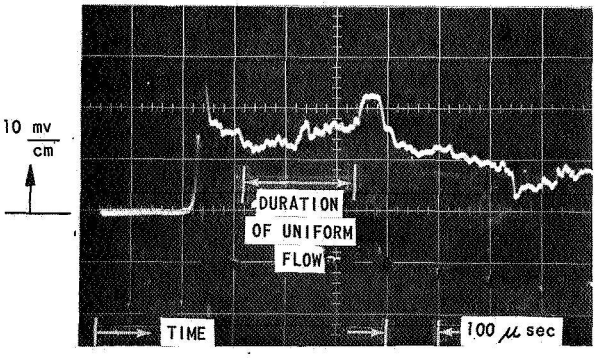

(e) CENTERLINE LANGMUIR PROBE OUTPUT (ACROSS 100Ω RESISTOR) AT 26.4" FROM THROAT (+3 VOLT BIAS)

DRIVER: 4000 psi H_2 (760°F)
DRIVEN: 10.0 mmHg NITROGEN
END-WALL MACH NO. : 9.8

Figure 36 INFLUENCE OF DRIVEN-TUBE GAS ON NOZZLE RADIATION INTENSITY AND ELECTRON-DENSITY MEASUREMENTS